

1
2
3
4
5
6
7
8
9
10
11
12
13
14
15
16

ETHANE IN PLANETARY AND COMETARY ATMOSPHERES:

TRANSMITTANCE AND FLUORESCENCE MODELS OF THE ν_7 BAND AT 3.3 μm

G. L. Villanueva^(1,2)

M. J. Mumma⁽¹⁾

K. Magee-Sauer⁽³⁾

⁽¹⁾ Solar System Exploration Division, Mailstop 690.3, NASA Goddard Space Flight Center, Greenbelt, MD, 20771, USA. Geronimo.Villanueva@nasa.gov
⁽²⁾ Department of Physics, Catholic University of America, Washington, DC 20064.
⁽³⁾ Department of Physics and Astronomy, Rowan University, Glassboro, NJ 08028.

Submitted to JGR Planets on December/22/2010

Revised April/21/2011

Accepted May/9/2011

1 **Abstract**

2 Ethane and other hydrocarbon gases have strong ro-vibrational transitions in the 3.3 μm
3 spectral region owing to C-H, CH₂, and CH₃ vibrational modes, making that spectral
4 region prime for searching possible biomarker gases in extra-terrestrial atmospheres (e.g.
5 Mars, exoplanets) and organic molecules in comets. However, removing ethane spectral
6 signatures from high-resolution terrestrial transmittance spectra has been imperfect,
7 because existing quantum mechanical models have been unable to reproduce the
8 observed spectra with sufficient accuracy. To redress this problem, we constructed a line-
9 by-line model for the ν_7 band of ethane (C₂H₆), and applied it to compute telluric
10 transmittances, and cometary fluorescence efficiencies. Our model considers accurate
11 spectral parameters, vibration-rotation interactions, and a functional characterization of
12 the torsional hot-band. We integrated the new band model into an advanced radiative
13 transfer code for synthesizing the terrestrial atmosphere (LBLRTM), and achieved
14 excellent agreement with transmittance data recorded against Mars using three different
15 instruments located in the Northern and Southern hemispheres. The retrieved ethane
16 abundances demonstrate the strong hemispheric asymmetry noted in earlier surveys of
17 volatile hydrocarbons. We also retrieved the sensitive limits to the abundance of ethane
18 on Mars. The most critical validation of the model was obtained by comparing
19 simulations of C₂H₆ fluorescent emission with spectra of three hydrocarbon-rich comets:
20 C/2004 Q2 (Machholz), 8P/Tuttle, and C/2007 W1 (Boattini). The new model accurately
21 describes the complex emission morphology of the ν_7 band at low rotational temperatures
22 and greatly increases the confidence of the retrieved production rates (and rotational
23 temperatures) with respect to previously available fluorescence models.

1. Introduction

Ground-based infrared astronomy is a powerful tool for characterizing molecular compositions of cometary and planetary atmospheres. In the 1990's, advances in infrared detectors enabled scientists to study bright infrared lines in comets and planets and to characterize their chemical compositions with unprecedented sensitivity. In 1999, commissioning of the first cross-dispersed infrared spectrometer at a large aperture telescope (NIRSPEC at Keck-2, McLean et al. 1998) closed the century that saw infrared spectroscopy transition from single element thermopiles behind low-resolution spectrographs to million-pixel detector arrays behind high-resolution spectrometers that span the entire 1-5 μm wavelength range. Similar instruments followed quickly at other giant telescopes, together driving a revolution in molecular astronomy. The higher sensitivities and improved spectral resolution of these instruments have highlighted the limitations of current models for analyzing spectra acquired with them, and have revealed ancillary issues introduced by incomplete and/or incorrect molecular parameters. The latter problem is especially acute in the important near infrared spectral region where all aliphatic and aromatic hydrocarbons have infrared-active vibrational modes.

Hydrocarbon gases have strong ro-vibrational transitions in the 3.3 μm spectral region owing to C-H, CH_2 , and CH_3 vibrational modes, making that spectral region prime for searching possible biomarker gases in extra-terrestrial atmospheres (e.g., Mars, exoplanets) and organic molecules in comets. For example, ethane has strong ν_7 and ν_5 fundamental bands with origins at wavelengths (frequencies) near 3.35 μm (2985 cm^{-1}) and 3.45 μm (2896 cm^{-1}), respectively. The discovery of abundant ethane in comet C/1996 B2 (Hyakutake) [Mumma et al. 1996], and its detection in every comet sampled

1 since then [DiSanti and Mumma 2008, Mumma & Charnley 2011, and refs. therein],
2 created a need for accurate models of solar-pumped fluorescence for these two
3 vibrational bands. A simple initial model for the four Q-branches seen in Hyakutake was
4 soon extended to account for the increased number of Q-branches observed in C/1995 O1
5 (Hale-Bopp) [Dello Russo et al 2001]. The rapid increase in power of cross-dispersed and
6 high resolution infrared spectrometers (NIRSPEC in 1999, CRIRES in 2005) soon
7 revealed even more spectral lines of ethane ν_7 [Mumma et al. 2001, Dello Russo et al.
8 2006] and stimulated the first systematic study of ν_5 [Radeva et al. 2011], in comets and
9 in Earth's atmosphere. However, the incomplete or improper accounting of ethane in
10 public spectral databases seriously constrained the accuracy of models for telluric
11 transmission and thus limited the achievable sensitivities for data taken using ground-
12 based telescopes.

13 In this paper, we present a complete quantum mechanical model for the ro-vibrational ν_7
14 band of ethane (C_2H_6), using more accurate spectral parameters. We next discuss the
15 limitations of molecular databases and models for synthesizing telluric atmospheric
16 transmittance and the solar spectrum, and we present improved models for this purpose.
17 We then obtain new line-by-line fluorescence efficiencies for ethane in space by coupling
18 the new ν_7 band model with the solar spectrum (including Fraunhofer lines). Finally, we
19 synthesize the terrestrial transmittance spectrum using improved molecular parameters
20 (including ethane ν_7). We illustrate the increases in accuracy and sensitivity achieved, by
21 applying these models to ground-based spectra of Mars and of comets [C/2004 Q2
22 (Machholz), 8P/Tuttle, and C/2007 W1 (Boattini)].

2. The Ethane model

HITRAN is a comprehensive database of molecular parameters that is widely used by the spectroscopic community for synthesizing and analyzing spectra of atmospheric gases. The database undergoes regular updates and additions, and its completeness has improved greatly in recent years. The latest version [Rothman et al. 2009] contains almost 3 million lines from 42 molecules, yet the database is still not sufficient in some spectral regions. Ethane provides a good example. Even though C_2H_6 is present in the terrestrial atmosphere at only trace amounts (0.1–2 ppbv), the lines of its strongest band (ν_7) are prominent in high-resolution atmospheric spectra. The latest HITRAN distribution includes parameters for some Q- branches derived by Brown et al. [1987] from ATMOS spectra, with later improvements for the PQ_3 sub-band from Pine and Rinsland [1999]. P- and R-branch lines are not listed. Here, we present a complete quantum mechanical band model for the ν_7 band, including lines of P-, Q-, and R- branches.

2.1. The ro-vibrational structure

For decades, laboratory scientists have extensively studied the ro-vibrational bands of C_2H_6 , but due to the complex morphology of the ethane bands and strong spectral confusion only a limited set of spectroscopic constants have been retrieved. Ethane is composed of two methyl groups in which H-atoms of the CH_3 groups are sterically staggered by 60° about the C-C axis of three-fold symmetry). The molecule has twelve fundamental vibrations involving C-H and C–C stretching (ν_1 , ν_3 , ν_5 , ν_7 , ν_{10}),

1 deformation of the methyl group ($\nu_2, \nu_6, \nu_8, \nu_{11}$), torsion (ν_4), and bending (ν_9, ν_{12}). The
 2 perpendicular band at $3.3 \mu\text{m}$ (ν_7) is infrared active and originated by stretching of the C-
 3 H bonds of individual methyl groups (see Fig. 1a). The characterization of rotational
 4 structure in this complex molecule is non-trivial because the ν_7 band is severely perturbed
 5 by overtones and combination states (with a low frequency torsional mode (ν_4) at ~ 289
 6 cm^{-1}) that are in Fermi or Coriolis resonance with ν_7 [Pine and Lafferty, 1982]. For some
 7 K sub-bands (e.g., RQ_5) the perturbations are so severe that the energy levels cannot be
 8 simply described using a standard power series expansion [Pine and Lafferty, 1982].

9 Description of the energy levels was performed using linear progressions of J, K and ℓ
 10 (where " denotes lower state and ' upper state). Considering that C_2H_6 is a prolate
 11 symmetric top molecule, the quantum numbers J and K respectively indicate the total
 12 angular momentum of the molecule and its projection onto the symmetry-axis, thus $K \leq J$
 13 (see Fig. 1b). For the ground vibrational state (see Fig. 1c) we applied the constants
 14 compiled by Pine and Lafferty 1982 (summarized in Table 1) in the form of:

$$15 \quad E''(J'', K'') = (A - B)K''^2 + BJ''(J'' + 1) - D_J J''^2 (J'' + 1)^2 - D_{JK} J''(J'' + 1)K''^2 - D_K K''^4 \quad (1)$$

16 We have had success using this simple progression for most sets of lines, but have
 17 encountered problems when trying to match the P-, R-, and Q-lines of $K \ell'' = 0$ ($\Delta K = 1$).
 18 This difficulty indicates the limitations of this simple approximation, and a more detailed
 19 and complete model of the energies for the ground state is required to correctly model all
 20 fundamental bands of ethane. We have provisionally circumvented this problem by
 21 defining a different set of upper-state rotational constants for $\Delta J = 0$ and $\Delta J \neq 0$ for $K \ell' = 1$
 22 [see Table 1].

For the upper state, Goldman et al. [1989] obtained a relatively accurate set of rotational constants for each K-ladder using high-resolution spectra recorded by Cole et al. [1980] and Pine and Lafferty [1982]. As described by Goldman et al. [1989], this power series approximation of J and K does not fully characterize the complexity of the ν_7 band, but it does achieve a reasonable precision of 0.004 to 0.010 cm^{-1} in frequency (see Table 2 of [Goldman et al. 1989]) for a limited number of lines. In 1996, Pine and Stone [1996] provided refined rotational constants for a limited set of Q-lines of RQ_0 , PQ_3 and RQ_3 (including splittings by torsional tunneling and A_1 - A_2 doublings). More recently, Harrison et al. [2010] have obtained high-resolution line strengths (cross sections) for ethane in the 3 μm region at temperatures between 194 and 297K and total pressures from 0.0689 Torr to 763.48 Torr. Using this dataset we identified 466 lines, which we consolidated with 122 lines reported by Dang-Nhu et al. [1984] and 66 observed by Pine and Stone [1996], ultimately deriving rotational constants for 30 K-ladders [see Table 1] of the ν_7 band of ethane. The upper state energies are calculated following:

$$E'(J', K\ell') = F'_{K\ell'} + B'_{K\ell'} J'(J'+1) - D'_{K\ell'} J'^2 (J'+1)^2 + H'_{K\ell'} J'^3 (J'+1)^3 + T_{K\ell'}(J') \quad (2)$$

where the F, B, D and H coefficients were fitted for each K-ladder using the compilation of lines reported above. We retrieved the third order coefficient (H) only when the precision of line frequencies was sufficient to quantify this parameter. For some K-ladders we observe strong perturbations, which cannot be described using a simple linear progression. These perturbations were described using the following formula:

$$T_{K\ell'}(J') = P1_{K\ell'} \cdot (J' - P2_{K\ell'}) \cdot \exp(P3_{K\ell'} \cdot |J' - P2_{K\ell'}|) \quad (3)$$

where P1, P2 and P3 are the perturbation coefficients summarized in Table 1. A representation of these perturbations for RQ_2 is presented in Figure 2. For lines beyond $K\ell' < -8$ and $K\ell' > 10$, we neglect the T and H terms of equation 3, and describe the energy origins (F) and effective rotational constant (B) following Goldman et al. [1989] with:

$$F' = \nu_0 - 2(A\zeta)'K'\ell' + (A' - B')K'^2 - D'_K K'^4 + \eta'_K K'^3 \ell' \quad (4)$$

$$B' = B_0 - D'_{JK} K'^2 + \eta'_J K\ell' \quad (5)$$

in which the parameters [see values in Table 1] were fitted to all identified lines, with the exception of lines accessing $K'' = 4, 5, 6$ which appear to be especially perturbed.

Using this energy model, we obtained a standard deviation of 0.005 cm^{-1} for 654 lines with quantum numbers: $-8 \leq K\ell' \leq 10$, and $J' \leq 28$ (see Figure 2). These solutions do provide good results for the selected lines, but because of the numerous perturbations their validity for higher quanta and weaker spin species is uncertain. The use of individual constants for each K-ladder provides a major advance (see spectra in Figure 3), corresponding to a 36-fold improvement with respect to the 0.18 cm^{-1} standard deviation obtained using a single progression (equations 4 and 5) with the global factors in Table 1, and a 50-fold improvement to the 0.25 cm^{-1} standard deviation obtained using the global constants provided by Goldman et al. [1989]; see comparison in Figure 2.

2.2 Spin symmetries and spin temperature

The characterization of the unique symmetries in the ethane molecule is particularly confusing, especially because different authors consider different notations depending on the assumed point group model. If internal rotation tunneling is neglected, the symmetries of the levels can be described with a point group D_{3d} (staggered) model having three spin modifications (A_1 , A_2 , E) with 'g' and 'u' notations. In cases where torsional tunneling leads to noticeable splittings, the symmetries are best described with the G_{36}^+ permutation-inversion group having seven different symmetries (A_{1s} , A_{4s} , E_{1s} , E_{2s} , E_{3s} , E_{4s} , G_s). Symmetries of rotational levels in the ground and ν_7 vibrational states are presented in Table 1 for both point groups, including statistical weights (w'' and w'). Because both notations use similar letters (A , E), the reader should be careful not to confuse these definitions when examining previous publications. In this paper, we make use of both notations and distinguish between these definitions by preserving the spin label subscripts ('g' and 'u' for the D_{3d} model, and 's' for the G_{36}^+ model). Lines are only permitted between $A \leftrightarrow A$, $E \leftrightarrow E$ and $G \leftrightarrow G$ levels (for both notations), and thus exchange between different spin species is normally considered negligible.

The spin ratios (or equivalent spin temperature, see Figure 4) can be related to the formation conditions of the molecule, and ultimately be used as a cosmogonic indicator. Unfortunately little is known about the interconversion of spin states in molecules with such high dimensional symmetry. A similar molecule (C_2H_4) was studied by Sun et al. [2005], who observed conversions among nuclear spin isomers but no exchange in the inversion symmetry. But in the case of ethane, its molecular symmetry group does not have a unique element relating to inversion in space, as nicely summarized by Hougen

and Oka [2005]. Thus, the relationship between spin ratio at formation and after elapsed times of order billions of years is uncertain; further studies will be required to properly assess this property of the ethane molecule. As shown in Figure 4, the relationship between E_g/A_g becomes equilibrated at very low temperatures ($>10K$), much lower than for the curves of H_2O , NH_3 and CH_4 .

2.3. Line intensities

The selection rules for the ν_7 band of ethane are: $\Delta J = J' - J'' = +1, 0, -1$; $\Delta K = K' - K'' = \ell' = +1, -1$, and $A \leftrightarrow A$, $E \leftrightarrow E$, $G \leftrightarrow G$. Line intensities S_v [cm^{-1} (molecule cm^{-2}) $^{-1}$] between allowed upper and lower states with $K'' < 20$ and $J'' < 50$ were computed as following:

$$S_v(T) = (\nu/\nu_0) S_v^0(T) L_{HL}(J'', K'', \Delta J, \Delta K) F_{HW}(J'', K'', \Delta J, \Delta K) SE(\nu) Pop(E'', w'', T) \quad (6)$$

where ν is the line frequency ($E' - E''$ [cm^{-1}]), ν_0 is the band center [cm^{-1}], S_v^0 is the band intensity [cm^{-1} (molecule cm^{-2}) $^{-1}$, see Table 1], L_{HL} is the Hönl-London factor, F_{HW} is the Herman-Wallis factor, SE is the stimulated emission factor and Pop is the fractional population of the lower state.

The Hönl-London factor (L_{HL}) for a perpendicular band ([Herzberg 1945, p426], $\Delta J = J' - J''$, m_L is 4 for $K'' \neq 0$ or 2 for $K'' = 0$) is calculated as:

$$\begin{aligned} \Delta J = 1 \quad L_{HL}(J'', K'', \Delta K) &= \frac{(J'' + 2 + K'' \Delta K)(J'' + 1 + K'' \Delta K)}{m_L(J'' + 1)(2J'' + 1)} \\ \Delta J = 0 \quad L_{HL}(J'', K'', \Delta K) &= \frac{(J'' + 1 + K'' \Delta K)(J'' - K'' \Delta K)}{m_L J''(J'' + 1)} \\ \Delta J = -1 \quad L_{HL}(J'', K'', \Delta K) &= \frac{(J'' - 1 - K'' \Delta K)(J'' - K'' \Delta K)}{m_L J''(2J'' + 1)} \end{aligned} \quad (7)$$

1 The Herman-Wallis factor (F_{HW}) corrects for vibration-rotation interactions, since the
 2 effective dipolar operator of a molecule (and thus the intensity of a spectral line) depends
 3 not only on the total angular momentum but on vibrational operators as well. The
 4 Herman-Wallis factor was calculated as:

$$5 \quad F_{HW}(J'', K'', \Delta J, \Delta K) = \left[1 + \alpha K'' \Delta K + \beta \Delta J \left(J'' + \frac{1}{2} + \frac{\Delta J}{2} \right) + \dots \right]^2 \quad (8)$$

6 where α and β are the coefficients presented in Table 1. Stimulated emission is described
 7 with $SE(\nu) = [1 - \exp(-\nu hc/kT)]$, and the relative population as $Pop(w'', E'', T) = w''$
 8 $\exp(-E''hc/kT) / Q_R(T)$, where hc/K is the second radiation constant and $Q_R(T)$ the
 9 rotational partition function at temperature T ($Q_R(296K) = 51617$).

10 The three spectroscopic parameters that describe the intensity of the ν_7 band (S_v^0 , α and
 11 β) were quantified by Dang-Nhu et al. [1984, 1987] to be $S_v^0(296K) = 349 \pm 4.6$
 12 $\text{cm}^{-2} \text{atm}^{-1}$, $\alpha = 0.0144 \pm 0.0012$ and $\beta = 0$ (assumed). We observe a change in the sign in
 13 the second term of the Herman-Wallis equation in Dang-Nhu et al. [1987] with respect to
 14 Dang-Nhu et al. [1984], implying a negative value of $\alpha = -0.0144$, that could be related to
 15 a misprint in [Dang-Nhu et al. 1987]. Using the latest cross-sections reported by Harrison
 16 et al. [2010] we retrieved $\alpha = 0.0096 \pm 0.0020$ and $\beta = -0.0034 \pm 0.0020$. Our value of α
 17 is within 2σ of that reported by Dang-Nhu et al. [1984].

18 The accuracy and precision of measurements of the total band intensity (S_v^0) are directly
 19 related to the considered calibration standards, and the scheme considered to mitigate for
 20 spectral confusion. The latter is particularly crucial for ethane near $3.3 \mu\text{m}$ since multiple
 21 fundamental (e.g. ν_7 and ν_5), combination (e.g. $\nu_8 + \nu_{11}$), and hot-bands (e.g. $\nu_7 + \nu_4 - \nu_4$)

overlap at these wavelengths (see Figures 3 and 6). Harrison et al. [2010] have gone to great extents to obtain accurate absorption cross sections for ethane at these wavelengths, with an overall uncertainty of 4%. Their cross-sections were calibrated against PNNL spectra (Pacific Northwest National Laboratory IR database, <http://nwir.pnl.gov>), which are now considered the gold standard for ethane. Considering these new absorption cross-sections and taking into account the first torsional hot-band (see details in section 2.6), we derived a S_v^0 of $301 \text{ cm}^{-2} \text{ atm}^{-1}$ for the ν_7 band, a correction of 14% with respect to the value previously reported by Dang-Nhu et al. 1984.

2.4 Einstein A_{21} coefficients

Einstein-A coefficients were computed following Šimečková et al. [2006]:

$$A_{21} = \frac{8\pi c \nu^2 Q_{\text{tot}}(T) S_v(T)}{[1 - \exp(-h\nu/kT)] [\exp(-E''/kT)] I_a w'} \quad (8)$$

where $Q_{\text{tot}}(T)$ is the total internal partition sum (TIPS, Fischer et al. 2003) ($TIPS = 70881$ at 296 with $Q_v(296) = 1.3732$), and I_a is the isotopic abundance ($I_a = 0.97699$ for normal C_2H_6).

2.5 Lineshape parameters

Malathy Devi et al. [2010a,b] reported an extensive and comprehensive study of line shape parameters (self- and N_2 -broadening half widths and their temperature dependence) for the ν_9 band (825 cm^{-1}) of ethane using a multispectrum analysis of data acquired at

1 PNNL and at the Jet Propulsion Laboratory (JPL). We applied the temperature
2 dependence of the broadening coefficients using constants reported in Table 2 of Malathy
3 Devi et al. [2010a] for $K'' \leq 9$ and half-width coefficients (self and N_2) from Table 5 of
4 Malathy Devi et al. [2010b] for $K'' \leq 3$. For lines accessing K'' higher than the available
5 measurements, we considered the mean progressions as presented in Figure 5. For
6 pressure-shifts we consider the N_2 -broadened pressure-induced shifts of $-0.004 \text{ cm}^{-1}/\text{atm}$
7 derived by Pine and Stone [1996] from RQ_0 and PQ_3 . A summary of the coefficients is
8 presented in Table 1.

9

10 **2.6. Torsional hot-bands**

11 Ethane has a low energy torsional mode (ν_4) with its first excited level at 289 cm^{-1} , and
12 thus hot-bands associated with this level ($\nu_X + \nu_4 - \nu_4$) are relatively prominent at
13 moderate temperatures. Spectroscopists have resorted to low temperatures and/or
14 extremely high-resolution laboratory experiments to minimize/remove the confusion of
15 hot and cold bands [e.g. Dang-Nhu et al. 1984, Pine & Stone 1996]. Using sub-Doppler
16 molecular-beam optothermal spectroscopy, Pine and Stone [1996] resolved the complex
17 structure of the PQ_3 , RQ_0 and RQ_3 sub-bands. Their measurements revealed new
18 absorption lines, which Pine and Rinsland [1999] attributed to a torsional hot band
19 ($\nu_7 + \nu_4 - \nu_4$, $E_g - A_{1u}$) with an intrinsic intensity (S_{vHOT}^0) of $\sim 80\%$ to that of the
20 fundamental (S_v^0). Considering equation 6, the band intensity measured by Pine and
21 Rinsland [1999] contributed $\sim 20\%$ ($80\%/4$) of the ν_7 band at 296K, if the summed
22 population in the first torsional level was one-fourth as large as that of the ground state at

1 296K. The hot band contribution is greatly reduced at cometary temperatures, and for
2 instance at 100K is only 1% if we assume that vibrational populations are thermally
3 equilibrated.

4 Unfortunately there are no spectral constants for the $\nu_7 + \nu_4 - \nu_4$ band, and Pine and
5 Rinsland [1999, Table 1] only provided coarse estimates for parameters of the hot
6 analogue of the PQ_3 sub-band by simulating the band contour observed by Pine and Stone
7 [1996]. The $\nu_7 + \nu_4$ -ground ($E_g - A_{1g}$) combination band is observable through Raman
8 spectroscopy, and was tentatively detected by Fernandez et al. [2003], although the low
9 signal to noise ratio limited the extraction of reliable rotational constants for the $\nu_7 + \nu_4$
10 vibrational level. Their measurements however predict the location of the hot-band to be
11 in the 2984-2950 cm^{-1} frequency range, consistent with the findings of Pine & Rinsland
12 [1999] and with our results (Figure 6).

13 We see strong extra absorption near the Q-branches of the ν_7 band (Figure 6a, b, c). We
14 investigated the temperature dependence of these features by integrating around (± 0.3
15 cm^{-1}) the strongest Q-branches, and observed that the ratio of data and model (Fig. 6d)
16 coincided with the vibrational partition function of the ν_7 level and its first torsional
17 component, confirming the origin of this absorption to be the $\nu_7 + \nu_4 - \nu_4$ hot-band. We
18 excluded the PQ_1 Q-branch from the analysis because it appeared slightly saturated in the
19 Harrison et al. [2010] dataset. Due to the strong spectral confusion and complexity of this
20 hot-band system, it is not yet possible to extract reliable constants for this hot-band
21 system.

At 296K, the observed intensity of the hot-band was 25% with respect to the fundamental $[\sum S\nu_{7\text{HOT}}(296\text{K})/\sum S\nu_7(296\text{K})]$, similar to the findings of Pine and Rinsland [1999] for the $^{\text{P}}\text{Q}_3$ replica of $\sim 20\%$ (see above). Perhaps, a technique as considered by Oomens and Reuss [1996] to study the $\nu_7+\nu_9-\nu_9$ hot-band of ethane should be employed to fully characterize the $\nu_7+\nu_4-\nu_4$ hot-band. We currently account for the existence of the hot-band in our moderate resolution spectra, by computing a simplistic $\nu_7+\nu_4-\nu_4$ line-list that considers the rotational constants of ν_4 from Blass et al. 1990 (neglecting torsional subspecies), and fitted constants for the $\nu_7+\nu_4$ using the data presented in Figure 6.

9

2.7. Machine readable spectral atlas

Following the above guidelines, we computed 17,266 spectral lines with $K_{\text{max}} = 20$ and $J_{\text{max}} = 40$ in the 2900 cm^{-1} to 3100 cm^{-1} frequency range; 8,680 for the ν_7 band and 8,586 for the hot-band. The database has been organized following the HITRAN 2008 format with line identifications following the G_{36}^+ point group model. To allow for future investigations of conversion efficiencies between different symmetries, we report lines for each symmetry individually, even if the lines are not resolved (e.g., a $A_{34s}-A_{12s}$ line is reported as two lines: $A_{3s}-A_{1s}$ and $A_{4s}-A_{2s}$). The vibrational indicators are V7, GROUND, V7+V4 and V4; while the local quantum numbers are J K and ℓ . The atlas for the ν_7 band has been provided to the HITRAN team for further integration into their consolidated database. Due to the large uncertainty in the rotational constants of the hot-band, we will only provide the atlas of the hot-band upon request, and to be used with moderate resolution spectra only.

3. Modeling of ethane in terrestrial atmospheres (LTE case)

Ground-based spectra of extraterrestrial and cometary atmospheres are affected by telluric absorption. The incoming spectral lines are often Doppler-broadened and they experience extinction by atmospheric lines that may themselves approach the Doppler-broadened limit (e.g., gases with significant stratospheric and mesospheric components, such as CH₄, CO₂, and O₃). Analysis of spectra measured for such lines requires that telluric transmittance be synthesized at sub-Doppler resolution (a spectral resolution of not more than 100 m/s, or 0.001 cm⁻¹ at 3000 cm⁻¹). We applied the new model for C₂H₆ (ν_7 and torsional hot-band) to synthesize terrestrial spectra using an advanced radiative transfer code for the terrestrial atmosphere that accesses a customized database of spectral constants from 42 molecules including C₂H₆ [see Fig. 7 and Appendix A].

Proper synthesis of terrestrial spectra requires line-by-line, layer-by-layer radiative transfer modeling of the atmosphere, in which the quality of the synthesized spectrum depends directly on the robustness of the used set of radiative transfer equations, the precision of the adopted spectroscopic constants, and the accuracy of the assumed atmospheric conditions (Fig. 8 - P(z), T(z), abundance profiles, and geometrical conditions). Until 2005 we used the Spectrum Synthesis Program (SSP, [Kunde and Maguire 1974]) accessing the HITRAN 1992 [Rothman et al. 1992] to compute terrestrial spectra. From 2005 until 2009, we used the more advanced GENLN2 v4 model [Edwards 1992], which provides highly realistic and Doppler-limited spectral synthesis of the terrestrial atmosphere. We improved the GENLN2 v4 model by providing a correction to properly account for spectral pressure-shifts, and introducing the capability to access the

1 latest HITRAN databases [Villanueva et al. 2008a]. However, GENLN 2 is no longer
2 supported by NCAR (National Center for Atmospheric Research).

3 In 2005, a new efficient line-by-line radiative transfer became available, the LBLRTM
4 (Line-By-Line Radiative Transfer Model) [Clough et al. 2005]). Perhaps, one the biggest
5 advantages of this code relative to GENLN2, is that it is highly optimized, allowing us to
6 increase the number of layers and the number of spectral points for the same computation
7 time, ultimately achieving a more realistic atmospheric solution. In addition, this code is
8 maintained by AER (Atmospheric and Environmental Research, Inc.) and has been (and
9 continues to be) extensively validated against atmospheric spectra from the ultraviolet to
10 the sub-millimeter. Even though the AER team provides a compiled spectral database to
11 use with its LBLRTM, we have preferred to instead use the more universally recognized
12 HITRAN atlas as the base for our radiative transfer modeling (using LBLRTM) with our
13 own corrections and updates tailored to our requirements [see Appendix A].

14 Using our updated spectral database and LBLRTM, we synthesized spectra for the
15 complete L-band [$2.8 - 4.2\mu\text{m}$, Fig. 7], with a spectral resolution of 0.0005 cm^{-1} and
16 consistent with a mean sampling power of ~ 5 million ($\lambda/\Delta\lambda$), or a velocity resolution of
17 60 m s^{-1} . This novel method has been successfully applied to calibrate and process
18 infrared spectra of planets [Figs. 9 and 10] and comets [Figs. 12, 13 and 14] taken with
19 several instrument/telescope combinations (see Section 5).

20 Even though we obtain very good results with our ethane ν_7 band model, the line list is
21 based on a restricted set of spectral constants and this ultimately leads to limited precision
22 and accuracy. These imprecisions could cause assignment of improper transmittance

1 values for some incoming ethane lines due to accidental overlap with Doppler-broadened
2 lines of stratospheric O₃. Further empirical studies will be needed to properly characterize
3 the complete structure of this band, including a full description of torsional tunneling
4 splittings, overtone perturbations, hot-bands, and A₁-A₂ doublings for all K sub-bands.
5 We intend to expand our model as more complete ethane line parameters are obtained.

6

7 **4. Modeling of ethane in cometary atmospheres (non-LTE case)**

8 The C₂H₆ ν_7 band is particularly bright in hydrocarbon-rich comets where efficient solar
9 pumping (and inefficient collisional quenching) leads to strong C₂H₆ fluorescence
10 emission. The complexity of the band in comets is revealed in Figures 12, 13 and 14. The
11 torsional mode is inactive to radiative decay and little is known about its possible
12 collisional quenching or excitation. It is possible that the vibrational partitioning (of ν_4)
13 imparted upon release at the cometary nucleus is maintained throughout the inner coma,
14 and thus the torsional manifold could become increasingly disequilibrated from the
15 rotational and kinetic distributions as the gas flows outward through the coma, ultimately
16 permitting pumping from the torsional level and leading to ν_7 hot-band fluorescent
17 emission. Our cometary data show no evidence of strong hot-band emission, but higher
18 spectral resolution and a better understanding of the spectral character of the hot-band
19 will be necessary to test its contribution or lack thereof to the total flux in the ν_7 region.

20 Collision partners in cometary atmospheres usually lack sufficient energy to excite
21 vibrational transitions and the rate of quenching collisions is much smaller than radiative
22 decay rates for (infrared active) excited states. Thus, the vibrational manifold is not

1 populated in LTE (local thermodynamic equilibrium). Instead, solar radiation pumps the
2 molecules into an excited vibrational state, which then de-excites by rapid radiative
3 decay. Infrared photons are emitted through decay to the ground vibrational state, either
4 directly (resonant fluorescence) or through branching into intermediate vibrational levels
5 (non-resonant fluorescence). Resonance fluorescence is the expected dominant factor in
6 the excitation and the sole pumping mechanism we consider here, although additional
7 excitation cascading from levels with energies higher than ν_7 may also be active. We
8 expect to expand the excitation for non-resonant fluorescence of the model, once
9 spectroscopic data of related bands become available.

10 Since fluorescence is a non-LTE process, computation of line-by-line fluorescence
11 efficiencies (g-factors) entails the building of a full quantum mechanical model. This
12 requires precise knowledge of the rotational structure (energy levels) for each vibrational
13 level involved, statistical weights, selection rules, perturbations (e.g. Coriolis effects,
14 splittings, tunneling) and band emission rates. The difficulty of this task has limited the
15 development of new models, particularly for those molecules having a complex
16 symmetry structure, and consequently only a limited set of line-by-line fluorescence
17 emission models are currently available. In the case of C_2H_6 , previous attempts to model
18 ν_7 fluorescence in comets focused only on integrated Q-branch intensities but did not
19 specify the fine rotational structure, aside from adopting a specific rotational temperature
20 [Mumma et al. 1996, Dello Russo et al. 2001].

21 Another problem with most current cometary (infrared) fluorescence models is that they
22 often assume the source for solar pumping is a simple black-body continuum with an
23 effective temperature of the Sun. This approximation is somewhat correct for the

1 continuum flux at certain wavelengths ($2900 - 3300 \text{ cm}^{-1}$), but it leads to inaccuracies
2 when computing pumping rates for individual ro-vibrational lines if the relative
3 heliocentric velocity of the comet shifts the pumping radiation field into solar absorptions
4 [Swings effect]. Omitting this effect will introduce not simply a relative error, but will
5 lead to incorrect retrievals of rotational and spin temperatures, since these are derived
6 from line-to-line intensity ratios. We replace the adopted blackbody radiation field with a
7 synthesis of the true solar spectra using a combination of empirical parameters from the
8 solar spectrum [Hase et al. 2006; 2010] calibrated with a stellar continuum flux model
9 [Kurucz 1997]; see Appendix B for a full discussion.

10 Fluorescence emission rates (g-factors) are normally quantified as energy (or quanta)
11 emitted per second per molecule in units of $[\text{J s}^{-1} \text{ molec}^{-1}]$, $[\text{W molec}^{-1}]$, $[\text{photon s}^{-1}$
12 $\text{molec}^{-1}]$ or simply $[\text{s}^{-1}]$, and are computed following a two-step process: 1) pumping to
13 the excited state and 2) relaxation to lower levels. The spectral constants needed to
14 compute g-factors can be extracted from an atlas of molecular lines, like HITRAN, if the
15 tabulated data are adequate. When validated, these databases are extremely valuable
16 repositories of the latest spectral constants and of line parameters that can be influenced
17 by complex perturbations such as Coriolis effects, splittings, resonances and tunneling.
18 Consequently we developed a General Fluorescence Model (GFM) to compute
19 fluorescence emission rates (see Appendix C), and applied it to our ethane line lists (hot
20 and cold ν_7 bands) by creating a complete atlas for this band system (as reported in
21 Section 2). Apart from C_2H_6 ν_7 (Table 1) and ν_5 (Radeva et al. 2011), we successfully
22 applied this approach to other infrared band-systems (ν_1 of HCN, ν_3 of CH_4 , 1-0 bands of
23 CO and ^{13}CO , ν_1 and $2\nu_2$ of HDO, ν_3 and $\nu_2+\nu_4+\nu_5$ of C_2H_2 , Villanueva et al. in prep.).

1

2 **5. Discussion of Models and Fluorescence Efficiency**

3 ***5.1. LTE Validation: Results from Ground-based Measurements***

4 We validate our synthetic terrestrial models by comparing them to infrared spectra of
5 Mars and comets acquired with different spectrometer/telescope combinations: CRIRES
6 (CRYogenic high-resolution InfraRed Echelle Spectrograph [Käufl et al. 2004]) at the
7 VLT (Very Large Telescope) in Chile, CSHELL (Cryogenic Echelle Spectrometer
8 [Tokunaga et al. 1990]) at the NASA-IRTF (InfraRed Telescope Facility) in Hawaii, and
9 NIRSPEC (Near-InfraRed Echelle SPECTrograph [McLean et al. 1998]) at the Keck II
10 Telescope in Hawaii.

11 In August 2009 we observed Mars using the CRIRES instrument, sampling the planet at
12 its mid-afternoon along meridian longitudes passing through Syrtis Major (an ancient
13 shield volcano) and the Hellas impact basin (geometry shown in Fig. 11a). These
14 observations reveal the recently discovered CO₂ band (Mars), multiple lines of water
15 (Mars, Earth), and the telluric absorption spectrum of the ν_7 band of C₂H₆ (Fig. 9). In
16 January 2006, we sampled Mars at its mid-morning along meridian longitudes passing
17 through Valles Marineris and the Argyre impact basin (geometry shown in Figs. 11b-c)
18 using two CSHELL settings obtained on two consecutive days (Fig. 10).

19 For each observatory, we synthesized terrestrial transmittance and radiance spectra for
20 C₂H₆ and other species by assuming default geometrical conditions for that high-altitude
21 site, assuming clear atmospheric conditions (no aerosols), 50 (optically thin) atmospheric
22 layers, and LTE populations. The atmospheric conditions (pressure, temperature and

1 abundances) are based on a standard tropical profile (Fig. 8), modified to describe the
2 observing conditions through two temperature parameters (T1 and T2), a pressure scaling
3 factor (PF) and abundance factors (AF, see profiles for CH₄ and C₂H₆ in Fig. 8c). The
4 given pressure profile is scaled following $P'(z) = P(z) \times PF$, while the temperature profile
5 is divided into tropospheric (affected by T1) and stratospheric (affected by T2, see Fig.
6 8a) sectors. The abundance profiles are scaled relative to the tropical profile by a
7 molecular multiplier relative to the tropical value. For each dataset, we retrieved
8 abundances and the atmospheric parameters (T1, T2, PF) using a Levenberg-Marquardt
9 non-linear-minimization algorithm that compares the transmittance model to the
10 absorption features observed against the planetary continua.

11 Agreement of the terrestrial ethane residuals and synthesized spectra is very good, and
12 reveals strikingly different C₂H₆ abundances at Mauna Kea in Hawaii and Cerro Paranal
13 in northern Chile. In particular, the CH₄ abundance was nominal for both sites, but the
14 C₂H₆ abundance showed important seasonal variations and extremely low values for the
15 Southern hemisphere. At first, we were concerned that inaccuracies of the ν_7 band model
16 introduced these excursions, but earlier independent investigations confirm our retrievals
17 [e.g. Rinsland et al. 2002, Glatthor et al. 2009]. For instance, the recent study of Helmig
18 et al. [2009] reports similar trends from a vast global monitoring program of volatile
19 organic compounds (VOCs), including C₂H₆. Both CH₄ and C₂H₆ mostly arise from
20 biogenic and anthropogenic emissions, although methane has a much longer lifetime (~8
21 years) than ethane (months, see Hough 1991) in the terrestrial atmosphere.

22 The short ethane lifetime causes important fluctuations in its atmospheric concentration,
23 since the sources and sinks vary geographically, and seasonally. This is particularly

1 evident in the Southern hemisphere where anthropogenic emissions are much smaller,
2 leading to a C_2H_6 maximum 7 times lower than in the Northern hemisphere [Helmig et al.
3 2009], consistent with our findings [see Table 2]. At the summit of Mauna Kea, we
4 observe an equivalent volume mixing ratio (VMR) of 1 ppb, similar to that of Rinsland et
5 al. [1994] (1.1 ppb) for Mauna Loa at this season. The retrievals from Rinsland et al.
6 [1994] were based on the ν_7 PQ_3 sub-branch of ethane, but ignored the presence of the
7 hot-band absorption from the $\nu_7 + \nu_4 - \nu_4$ band [Pine and Rinsland 1999] at these
8 frequencies. If we attempt to revise the values from Rinsland et al. [1994] considering
9 hot-band absorption and the new band intensity from PNNL spectra, their VMR would
10 become ~ 1 ppb, in excellent agreement with our results. These consistencies together
11 with the excellent agreement we obtained when we compared the synthetic models to
12 spectra taken using different instruments (Figs. 9, 10, 12, 13, 14) are important
13 validations of the ν_7 line-by-line model (including our updated spectral database) and the
14 radiative transfer modeling.

15 By properly accounting for the telluric absorption of C_2H_6 in this spectral region, we
16 obtain better quality residuals, ultimately allowing us to perform very sensitive searches
17 for biomarker gases on Mars and other astronomical objects. Using the residuals
18 presented in Figures 9 and 10, we obtained the most sensitive upper-limits for ethane on
19 Mars ever measured [see Table 2]. We can expect immediate improvement in these
20 upper limits by including additional spectral scans.

22 *5.2. Solar Spectrum: Extraterrestrial and Cometary Spectra*

1 The precise modeling of the solar spectrum is particularly important when observing
2 planetary bodies in reflected light (e.g., Mars, Moon). The infrared radiation observed
3 from Mars is a combination of reflected sunlight (with Fraunhofer lines) and planetary
4 thermal emission (featureless continuum). Sparse spectral lines of Mars' atmospheric
5 constituents are superposed on the continua according to the optical path experienced by
6 the two components [see Figs. 9 and 10]. Sunlight experiences a double optical path
7 (Sun-to-surface + surface-to-Observer), while the Mars "thermal" continuum traverses
8 only a single path (surface-to-observer). We determine the relative contributions of solar
9 and thermal emission to the measured continuum by comparing the measured area
10 (equivalent width) of Fraunhofer lines with their true value (see Appendix A). This
11 permits identification of the "effective" optical path needed to properly determine
12 molecular abundances on Mars (see details in Villanueva et al. 2008a, Novak et al. 2003),
13 and thus an accurate solar model has impact not only on the spectral residuals but also on
14 the retrieval process.

15 The signal-to-noise ratio (SNR) of the adopted solar spectrum limits the maximum
16 achievable quality of the residuals. At 3 μm the typical SNR of the ATMOS solar
17 spectrum [Abrams et al. 1996] is ~ 1000 (1σ), a sensitivity achievable in minutes with
18 most bright infrared sources (e.g., Mars, flux standard stars) using current high-resolution
19 spectrometers.

20 To increase the SNR of the residuals, we combined empirical and observational data from
21 ground-based and space-based instruments to obtain an improved model for the solar
22 spectrum (see Appendix B). This new solar spectrum will greatly contribute to the search
23 for weak spectral signatures within solar reflected sunlight; this is demonstrated with

Figs. 9 and 10, where we observe excellent agreement between the solar features imprinted in the Mars continua and those synthesized with the new solar model.

The precise description of solar features is of paramount importance when studying solar pumped fluorescence in comets. The use of a non-realistic solar pumping flux would introduce errors up to 30% for certain g-factors of the ν_7 band of C_2H_6 , and up to 40% for selected lines of the 1 – 0 band of CO, for example. Because this (Swings) effect is dependent on the heliocentric velocity of the comet, fluorescence rates need be computed for each orbital situation using the synthesized solar spectrum described in equation C-3.

5.3. Validation of Fluorescence Efficiency Factors - Comets

We have chosen three cometary datasets (8P/Tuttle, C/2007 W1 (Boattini), C/2004 Q2 (Machholz)) to test the new C_2H_6 fluorescence model. These comets displayed bright ethane emissions and different rotational temperatures, in spectra acquired with CRIRES and NIRSPEC. Comet 8P/Tuttle (8P hereafter) was observed in Jan-Feb 2008 using CRIRES at the VLT with the adaptive optics (AO) system [Fig. 12]. Using AO minimizes slit-losses and achieves an increased signal-to-noise in the central part of the coma. The spatial resolution along the slit is high as well and is close to the diffraction limit of the telescope.

Results for six volatiles including C_2H_6 were presented in Böhnhardt et al. [2008]. At the time of observations (26 January 2008), the cometary ephemerides were: $r_h = 1.03$ AU (heliocentric distance), $v_h = -0.37$ km s⁻¹ (heliocentric velocity of the comet), $\Delta = 0.49$ AU (geocentric distance), $v = 24.7$ km s⁻¹ (geocentric velocity of the comet); and (as

1 retrieved from 19 water lines) the nucleus-centered rotational temperature was 60^{+8}_{-9} K
2 for H₂O. We synthesized a fluorescence model for C₂H₆ for the above mentioned
3 conditions, and retrieved a C₂H₆ production rate of $(1.74 \pm 0.06) \times 10^{26}$ molecules s⁻¹ for
4 8P, an improvement in the confidence limits of a factor of 3 (see Fig. 15) with respect to
5 the previously reported value derived with the old ethane fluorescence model (see Table
6 1 and Böhnhardt et al. [2008]).

7 A similar improvement was obtained with spectra of comet C/2004 Q2 (Machholz) (Q2
8 hereafter), which was observed using NIRSPEC in November 2004 and January 2005
9 [Bonev et al. 2009]. We applied the new C₂H₆ model to the spectra taken on 19 January
10 2005 [Fig. 13] and retrieved a production rate of $(13.3 \pm 0.25) \times 10^{26}$ mol s⁻¹ at 93K (a
11 correction of -12% to the value for T_{rot} reported previously) with a confidence limit
12 improved by a factor of 3. Considering a Q(H₂O) of $(2.727 \pm 0.070) \times 10^{29}$ mol s⁻¹ as
13 reported by Bonev et al. [2009] for this date, this would correspond to an ethane mixing
14 ratio of 0.488 ± 0.016 %. This mixing ratio is consistent with that derived from the ν_5
15 band of ethane for November 28 2004 by Radeva et al. [2011] of 0.48 ± 0.06 %. Lastly,
16 comet C/2007 W1 (Boattini) (W1 hereafter) was observed in July 2008 using NIRSPEC
17 [Fig. 14]. The comet has a particularly rich chemistry, and the ethane Q-branches are
18 very bright in our spectra. From the co-measured water spectrum and considering 20 lines
19 of H₂O, we retrieved a rotational temperature of 79 ± 3 K for H₂O on 9 July 2008 (see
20 details in Villanueva et al., in prep.). The C₂H₆ production rate for W1 at 79K is $(2.35 \pm$
21 $0.02) \times 10^{26}$ mol s⁻¹. For the three comets, we measured E_g/A_g ratios to be consistent with
22 equilibrium (T_{spin} > 10K).

1 As shown in Figs. 12, 13, 14 and 15, the new model shows excellent line-by-line
2 agreement with the cometary datasets, ultimately allowing us to extract improved
3 cometary abundances [see Table 2]. The new model also has led to improved
4 understanding of this complex spectral region, where many other hydrocarbons have
5 strong spectral signatures (e.g., methanol (CH_3OH), methane (CH_4) and ethylene (C_2H_4)).

6 The improvement of the C_2H_6 fluorescence model is attributed to differences between the
7 old [Dello-Russo et al. 2001] and new models arising from four aspects: 1) the previous
8 model did not properly account for the symmetries of ℓ -splitting of rotational levels of
9 the ν_7 vibrational level, leading to incorrect ro-vibrational branching ratios; 2) we
10 introduced updated molecular constants, partition functions, and performed a line-by-line
11 analysis (instead of a temperature independent “g-band” analysis); 3) we included the
12 complete fine rotational structure (P, Q, and R-branches) of the ν_7 band (including hot-
13 bands) leading to an overall increase in the considered flux integrated within each Q-
14 branch; and 4) the new model considers a realistic solar pumping spectrum.

16 **6. Conclusions**

17 We constructed a line-by-line model for the ν_7 band of ethane (C_2H_6), and applied it to
18 compute telluric transmittances, and cometary fluorescence efficiencies. The complex
19 and dense rotational fine structure of the ν_7 band system was described using a set of
20 accurate rotational constants for each K-ladder, including torsional hot-bands. The new
21 band systems were integrated into an advanced radiative transfer model of the terrestrial
22 atmosphere (LBLRTM), considering a rigorous line-by-line, layer-by-layer radiative

transfer analysis and including realistic atmospheric conditions, abundance profiles, and geometrical conditions. In addition to adding 17,266 ethane lines (ν_7 and $\nu_7 + \nu_4 - \nu_4$) to the spectral database accessed by the terrestrial model, we updated and expanded the CO₂ database by including our latest discoveries in the Martian atmosphere. Using these new models, we achieved excellent agreement with transmittance and fluorescence emission data recorded near 3.3 μm using three different instruments located in the Northern and Southern hemispheres.

We computed cometary fluorescence emission rates for a wide range of rotational temperatures (10-200K), and successfully validated the model by comparing it to measured spectra of three comets (C/2007 W1 (Boattini), C/2004 Q2 (Machholz) and 8P/Tuttle). The model makes use of a novel approach to synthesize the solar pumping, which combines a theoretical continuum model and a highly precise solar line list. The methodology used to calculate cometary fluorescence emission rates was standardized to extract information from existing spectral databases on C₂H₆ as well as all other molecules in the HITRAN database, and so is readily available to compute cometary fluorescence emission rates for multiple other molecules.

Acknowledgements

GLV acknowledges support from NASA's Planetary Astronomy Program (08-PAST08-0034) and NASA's Planetary Atmospheres Program (08-PATM08-0031). MJM was supported by NASA's Planetary Astronomy Program (RTOP 344-32-07) and NASA's Astrobiology Program (RTOP 344-53-51). KMS was supported by the Planetary

Astronomy RUI program of the National Science Foundation. We thank Dr. Hans-Ulrich Käufl for assisting with the Mars (CRIRES) observations in 2009, and Dr. Robert Novak and Dr. Avram M. Mandell for assisting with the acquisition of Mars (CSHELL) data in 2006. We thank the staff of the VLT Observatory, (operated by ESO), of the W. M. Keck Observatory (operated as a scientific partnership among CalTech, UCLA, and NASA), and of NASA's InfraRed Telescope Facility (operated for NASA by the University of Hawaii) for their exceptional support throughout our long Mars and cometary observing Programs. The authors wish to recognize and acknowledge the very significant cultural role and reverence that the summit of Mauna Kea has always had within the indigenous Hawaiian community. We are most fortunate to have the opportunity to conduct observations from this mountain.

References

- Abrams, M.C., Goldman, A., Gunson, M. R., Rinsland, C. P., Zander, R. (1996), Observations of the infrared solar spectrum from space by the ATMOS experiment, *Applied Optics*, vol. 35 pp. 2747.
- Anderson, G.P., Clough, S.A., Kneizys, F.X., Chetwynd, J.H., and Shettle, E.P. (1986). AFGL Atmospheric Constituent Profiles (0-120 km), *AFGL-TR-86- 0110*, Air Force Geophysics Laboratory, Hanscom AFB MA, 43 pp.
- Blass, W.E., Halsey G.W., Susskind J., Reuter D.C., Jennings D.E. (1990), Rotational parameters of the first torsional state of ethane from lower state combination differences in $\nu_9 + \nu_4 - \nu_4$, *J. Mol. Spectrosc.*, vol. 141 pp. 334.
- Bönnhardt, H., Mumma, M. J., Villanueva, G. L., DiSanti, M. A., Bonev, B. P., Lippi, M., Käufl, H. U. (2008), The Unusual Volatile Composition of the Halley-Type Comet 8P/Tuttle: Addressing the Existence of an Inner Oort Cloud, *Astrophys. J.*, vol. 683 pp. L71.
- Bonev, B. P., Mumma, M. J., Gibb, E. L., DiSanti, M. A., Villanueva, G. L., Magee-Sauer, K., Ellis, R. S. (2009), Comet C/2004 Q2 (Machholz): Parent Volatiles, a Search

1 for Deuterated Methane, and Constraint on the CH₄ Spin Temperature, *Astrophys. J.*, Vol.
2 699 pp. 1563.

3
4 Brown, L. R., Farmer, C. B., Rinsland, C. P. and Toth, R. A. (1987), Molecular line
5 parameters for the Atmospheric Trace Molecule Spectroscopy (ATMOS) Experiment, *Appl.*
6 *Opt.*, Vol. 26, 5154 - 5182.

7
8 Clough, S.A., Shephard, M.W., Mlawer, E.J., Delamere, J.S., Iacono, M.J., Cady-Pereira,
9 K., Boukabara, S., Brown, P.D. (2005), Atmospheric radiative transfer modeling: a
10 summary of the AER codes, *J. Quant. Spectrosc. Radiat. Transfer*, vol. 91 pp. 233.

11
12 Cole, A. R. H., Cross, K. J., Cugley, J. A., Heise, H. M. (1980), Infrared rotation-
13 vibration spectra of ethane . The perpendicular band ν_7 of C₂H₆, *J. Mol. Spectrosc.*, Vol.
14 83 pp. 233.

15
16 Crovisier, J., Encrenaz, T. (1983), Infrared fluorescence of molecules in comets - The
17 general synthetic spectrum, *Astron. Astrophys.*, vol. 126 pp. 170.

18
19 Dang-Nhu, M., Pine, A.S., Lafferty, W.J. (1984), Intensities in the ν_5 , ν_7 , and $\nu_8 + \nu_{11}$
20 bands of ethane ¹²C₂H₆, *Can. J. Phys.*, vol. 62 pp. 512.

21
22 Dang-Nhu, M., Goldman, A. (1987), Line parameters for C₂H₆ in the 3000 cm⁻¹ region, *J.*
23 *Quant. Spectrosc. Radiat. Transfer*, Vol. 38 pp. 159.

24
25 Dello Russo, N. D., Mumma, M. J., DiSanti, M. A., Magee-Sauer, K., Novak, R. (2001),
26 Ethane Production and Release in Comet C/1995 O1 Hale-Bopp, *Icarus*, 153, pp 162.

27
28 Dello Russo, N. D., Mumma, M. J., DiSanti M. A., Magee-Sauer, K., Gibb, E. L., Bonev,
29 B.P., McLean, I. S., Xu, L. (2006), A high-resolution infrared spectral survey of Comet
30 C/1999 H1 Lee, *Icarus*, vol. 184 pp. 255.

31
32 DiSanti, M.A., Mumma, M.J. (2008), Reservoirs for Comets: Compositional Differences
33 Based on Infrared Observations, *Space Sci. Rev.*, vol. 138 pp. 127.

34
35 Edwards, D. P. (1992), GENLN2: A general line-by-line atmospheric transmittance and
36 radiance model, Version 3.0 description and users guide, NCAR/TN-367-STR, *National*
37 *Center for Atmospheric Research*, Boulder, Co.

38
39 Gamache, R. R., Hawkins, R. L., Rothman, L. S. (1990), Total internal partition sums in
40 the temperature range 70-3000 K: Atmospheric linear molecules, *J. Mol. Spectrosc.*, vol.
41 142 pp. 205.

42
43 Glatthor, N., von Clarmann, T., Stiller, G.P., Funke, B., Koukouli, M.E., Fischer, H.,
44 Grabowski, U., Höpfner, M., Kellmann, S., Linden, A. (2009), Large-scale upper
45 tropospheric pollution observed by MIPAS HCN and C₂H₆ global distributions, *Atmos.*
46 *Chem. Phys.*, vol. 9 pp. 9619.

- 1 Goldman, A., Dang-Nhu, M., Bouanich J. P. (1989), Ethane 3 μm spectral clusters of
2 atmospheric interest, *J. Quant. Spectrosc. Radiat. Transfer*, Vol. 41 pp. 17.
3
- 4 Goldman, A., Gamache, R. R., Perrin, A., Flaud, J. M., Rinsland, C. P., Rothman, L. S.
5 (2000), HITRAN partition function and weighted transition-moments squared, *J. Quant.*
6 *Spectrosc. Radiat. Transfer*, Vol 66, 455–86.
7
- 8 Fernández, J.M., Montero, S. (2003), Torsional selection rules, Raman tensors, and cross
9 sections for degenerate modes of C_2H_6 , *J. Chem. Phys.*, vol. 118 pp. 2657.
10
- 11 Fiorenza C., Formisano V. (2005), A solar spectrum for PFS data analysis, *Planet. Space*
12 *Sci.*, Vol. 53 pp. 1009.
13
- 14 Fischer J., Gamache R. R., Goldman A., Rothman L. S., Perrin A. (2003), Total internal
15 partitions sums for molecular species on the 2000 edition of the HITRAN database, *J.*
16 *Quant. Spectrosc. Radiat. Transfer*, Vol 82, 401–12.
17
- 18 Harrison, J.J., Allen, N.D.C, Bernath, P.F. (2010), Infrared absorption cross sections for
19 ethane (C_2H_6) in the 3 μm region, *J. Quant. Spectrosc. Radiat. Transfer*, vol. 111 pp. 357.
20
- 21 Hase, F., Demoulin, P., Sauval, A. J., Toon, G. C., Bernath, P. F., Goldman, A.,
22 Hannigan, J. W., Rinsland, C. P. (2006), An empirical line-by-line model for the infrared
23 solar transmittance spectrum from 700 to 5000 cm^{-1} , *J. Quant. Spectrosc. Radiat.*
24 *Transfer*, vol. 102 pp. 450.
25
- 26 Hase, F., Wallace, L., Mcleod, S. D., Harrison, J. J., Bernath, P. F. (2010), The ACE-FTS
27 atlas of the infrared solar spectrum, *J. Quant. Spectrosc. Radiat. Transfer*, Vol. 111 (4)
28 pp. 521-528.
29
- 30 Helmig, D., Bottenheim, J., Galbally, I. E., Lewis, A., Milton, M. J. T., Penkett, S., Plass-
31 Duelmer, C., Reimann, S., Tans, P., Thiel, S. (2009), Volatile Organic Compounds in the
32 Global Atmosphere, *Eos Trans. Am. Geophys. Union*, vol. 90 pp. 513.
33
- 34 Herzberg, G. (1945), Molecular Spectra and Molecular Structure: II. Infrared and Raman
35 Spectra of Polyatomic Molecules, *Van Nostrand Inc.*, Princeton, New Jersey.
36
- 37 Hough, A. M. (1991), Development of a Two-Dimensional Global Tropospheric Model:
38 Model Chemistry, *J. Geophys. Res.*, 96(D4), 7325–7362.
39
- 40 Käufl, H., et al. (2004), CRIRES: a high-resolution infrared spectrograph for ESO's VLT.
41 Ground-based Instrumentation for Astronomy. Edited by Alan F. M. Moorwood and Iye
42 Masanori, *Proc. SPIE Int. Soc. Opt. Eng.*, vol. 5492 pp. 1218.
43
- 44 Kunde, V.R., Maguire, W.C. (1974). Direct integration transmittance model, *J. Quant.*
45 *Spectrosc. Radiat. Transfer*, vol. 14 pp. 803.
46

- 1 Kurucz R. L. (1997), The solar irradiance by computation. <http://kurucz.harvard.edu/>.
- 2
- 3 Malathy Devi, V., Benner, D.C., Rinsland, C.P., Smith, M.A.H., Sams, R.L., Blake, T.A.,
- 4 Flaud, J., Sung, K., Brown, L.R., Mantz, A.W. (2010a), Multispectrum measurements of
- 5 spectral line parameters including temperature dependences of N₂- and self-broadened
- 6 half-width coefficients in the region of the ν_9 band of ¹²C₂H₆, *J. Quant. Spectrosc. Radiat.*
- 7 *Transfer*, vol. 111 pp. 2481.
- 8
- 9 Malathy Devi, V., Rinsland, C.P., Benner C.D., Sams, R.L., Blake, T.A. (2010b),
- 10 Multispectrum analysis of the ν_9 band of ¹²C₂H₆: Positions, intensities, self- and N₂-
- 11 broadened half-width coefficients, *J. Quant. Spectrosc. Radiat. Transfer*, vol. 111 pp.
- 12 1234.
- 13
- 14 McLean, I.S., et al. (1998), Design and development of NIRSPEC: a near-infrared echelle
- 15 spectrograph for the Keck II telescope, *Proc. SPIE Int. Soc. Opt. Eng.*, Vol. 3354, pp.
- 16 566.
- 17
- 18 Mumma, M. J., DiSanti, M. A., Dello Russo, N. D., Fomenkova, M., Magee-Sauer, K.,
- 19 Kaminski, C.D., Xie, D.X. (1996), Detection of Abundant Ethane and Methane, Along
- 20 with Carbon Monoxide and Water, in Comet C/1996 B2 Hyakutake: Evidence for
- 21 Interstellar Origin, *Science*, vol. 272 pp. 1310.
- 22
- 23 Mumma, M. J. et al. (2001), A Survey of Organic Volatile Species in Comet C/1999 H1
- 24 (Lee) Using NIRSPEC at the Keck Observatory, *Astrophys. J.*, vol. 546 pp. 1183.
- 25
- 26 Mumma, M.J., Charnley, S. B. (2011), *Annu. Rev. Astron. Astr.*, under review.
- 27
- 28 Oomens, J., Reuss, J. (1996), The ν_7^+ ν_9^- ν_9 Hot Band in Ethane, *J. Mol. Spectrosc.*, vol.
- 29 177 pp. 19.
- 30
- 31 Pine, A. S., Lafferty, W. J. (1982), Torsional Splittings and Assignments of the Doppler-
- 32 Limited Spectrum of Ethane in the C-H Stretching Region, *J. Res. Nat. Bur. Stand.*, vol.
- 33 83 (3) pp. 1-20.
- 34
- 35 Pine, A. S., Rinsland, C. P. (1999), The role of torsional hot bands in modeling
- 36 atmospheric ethane, *J. Quant. Spectrosc. Radiat. Transfer*, vol. 62 pp. 445.
- 37
- 38 Pine, A. S., Stone, S. C. (1996), Torsional Tunneling and A₁-A₂ Splittings and Air
- 39 Broadening of the ^RQ₀ and ^PQ₃ Subbranches of the ν_7 Band of Ethane, *J. Mol. Spectrosc.*,
- 40 vol. 175 pp. 21.
- 41
- 42 Radeva, Y.L., Mumma, M. J., Villanueva, G. L., A'Hearn, M. F. (2011), A Newly
- 43 Developed Fluorescence Model for C₂H₆ ν_5 and Application to Cometary Spectra
- 44 Acquired with NIRSPEC at Keck II, *Astrophys. J.*, vol. 729 (2) pp. 135.
- 45

- 1 Rinsland, C.P., Goldman, A., Murcray, F.J., David, S.J., Blatherwick, R.D., Murcray,
2 D.G. (1994), Infrared spectroscopic measurements of the ethane (C₂H₆) total column
3 abundance above Mauna Loa, Hawaii - seasonal variations, *J. Quant. Spectrosc. Radiat.*
4 *Transfer*, vol. 52 pp. 273.
- 5
6 Rinsland, C.P., Jones, N.B., Connor, B.J., Wood, S.W., Goldman, A., Stephen, T.M.,
7 Murcray, F.J., Chiou, L.S., Zander, R., Mahieu, E. (2002), Multiyear infrared solar
8 spectroscopic measurements of HCN, CO, C₂H₆, and C₂H₂ tropospheric columns above
9 Lauder, New Zealand (45°S latitude), *J. Geophys. Res. Atmos.*, vol. 107 pp. 4185.
- 10
11 Rothman, L.S., et al. (2009), The HITRAN 2008 molecular spectroscopic database, *J.*
12 *Quant. Spectrosc. Radiat. Transfer*, vol. 110 pp. 533.
- 13
14 Rothman, L. S., Hawkins, R. L., Wattson, R. B., Gamache, R. R. (1992), Energy levels,
15 intensities, and linewidths of atmospheric carbon dioxide bands, *J. Quant. Spectrosc.*
16 *Radiat. Transfer*, vol. 48 pp. 537.
- 17
18 Šimečková, M., Jacquemart, D., Rothman, L.S., Gamache, R.R., Goldman, A. (2006),
19 Einstein A-coefficients and statistical weights for molecular absorption transitions in the
20 HITRAN database, *J. Quant. Spectrosc. Radiat. Transfer*, Vol. 98 pp. 130.
- 21
22 Snodgrass, H.B, Ulrich R.K (1990), Rotation of Doppler features in the solar
23 photosphere, *Astrophys. J.*, vol. 351 pp. 309.
- 24
25 Tobiska, W.K., Woods, T., Eparvier, F., Viereck, R., Floyd, L., Bouwer, D., Rottman, G.,
26 White, O.R. (2000), The SOLAR2000 empirical solar irradiance model and forecast tool,
27 *J. Atmos. Sol. Terr. Phys.*, 62, pp. 1233–1250
- 28
29 Tokunaga, A.T., Toomey, D.W., Carr, J., Hall, D.N.B., Epps, H.W. (1990), Design for a
30 1-5 micron cryogenic Echelle spectrograph for the NASA IRTF, *Instrumentation in*
31 *astronomy VII; Proceedings of the Meeting*, vol. 1235 pp. 131.
- 32
33 Vandaele, A.C, Villanueva, G. L., Bertaux, J. L., Borkov, Y., Drummond, R., Mahieux,
34 A., Montmessin, F., Mumma, M. J., Novak, R. E., Perevalov, V., Tashkun, S., Wilquet,
35 V. (2009), Updating CO₂ spectroscopic line list using Mars and Venus spectra,
36 International Conference on Comparative Planetology: Venus – Earth – Mars, *European*
37 *Space Agency, ESTEC*, Noordwijk, The Netherlands, 11- 15 May.
- 38
39 Villanueva, G. L., Mumma, M. J., Novak, R. E., Hewagama, T. (2008a), Identification of
40 a new band system of isotopic CO₂ near 3.3 μm: Implications for remote sensing of
41 biomarker gases on Mars, *Icarus*, vol. 195 pp. 34.
- 42
43 Villanueva, G. L., Mumma, M. J., Novak, R. E., Hewagama, T. (2008b), Discovery of
44 multiple bands of isotopic CO₂ in the prime spectral regions used when searching for CH₄
45 and HDO on Mars, *J. Quant. Spectrosc. Radiat. Transfer*, vol. 109 pp. 883.
- 46

- 1 Wallace, L., Livingston, W. (2003), An Atlas of the Solar Spectrum in the Infrared from
2 1850 to (1.1 to 5.4 microns), *revised. N.S.O. Technical Report #03-001*, National Solar
3 Observatory, Tucson.
4
5 Weaver, H.A., Mumma, M.J. (1984), Infrared molecular emissions from comets,
6 *Astrophys. J.*, Vol. 276 pp. 782.
7
8

Rotational constants for the ground state (Pine & Lafferty 1982)						
$A_0 = 2.671$ $B_0 = 0.6630271$ $D_0^K = 1.09 \times 10^{-5}$ $D_0^{JK} = 2.660 \times 10^{-6}$ $D_0^J = 1.0312 \times 10^{-6}$						
Rotational constants for the ν_7 vibrational state ^(a)						
$K \ell'$	Sym	F [cm ⁻¹]	B [cm ⁻¹]	D x 10 ⁻⁶ [cm ⁻¹]	Lines	r.m.s. [cm ⁻¹]
-8	A _s	3120.55085	0.66367616	1.6379	6	0.00083
-8	E _s	3120.57306	0.66354001	1.0500	4	0.00781
-7	E _u	3089.50468	0.66330074	0.7167	15	0.00749
-6	E _u	3062.67031	0.66214093	-2.0388	22	0.00632
-5	A _s	3039.18324	0.66383076	17.2659	19	0.00750
-5	E _s	3039.36507	0.66090799	-4.2371	10	0.00103
-4	E _u	3020.45860	0.66348953	2.1859	25	0.00699
-3	E _s	3005.61858	0.66348639	1.7780	11	0.01241
-3	G _s	3005.63978	0.66329109	1.2006	23	0.00344
-2	A _s	2994.84157	0.66312225	0.9459	14	0.00002
-2	E _s	2994.83990	0.66312201	0.9767	10	0.00005
-1	E _u	2988.09979	0.66303157	0.8945	36	0.00124
0	E _u	2985.38894	0.66303542	1.0141	22	0.00155
1	A _u ^(b)	2986.72474	0.66308908	1.0296	31	0.00245
1	A _s ^(c)	2986.72634	0.66289178	0.9789	14	0.00002
1	E _s ^(c)	2986.73272	0.66285832	1.1544	10	0.00004
2	E _s	2992.09430	0.66299073	1.2681	15	0.00241
2	G _s	2992.09721	0.66292818	1.0268	32	0.00644
3	E _s	3001.50382	0.66315921	1.4885	27	0.00776
3	G _s	3001.50571	0.66294774	0.9871	26	0.00428
4	A _s	3014.94266	0.66295652	0.9703	32	0.00111
4	E _s	3014.93730	0.66296202	1.0594	16	0.00047
5	E _u	3032.40473	0.66300958	0.8346	34	0.00127
6	E _u	3053.85189	0.66352169	0.6270	53	0.00565
7	A _u	3079.69389	0.65843003	-4.3470	41	0.00808
8	E _s	3108.98384	0.66162133	0.5372	19	0.00072
8	G _s	3108.98763	0.66150373	0.4632	38	0.00748
9	E _u	3142.50886	0.66190851	0.8715	16	0.00164
10	A _s	3180.03893	0.66210580	1.3212	22	0.00133
10	E _s	3180.03545	0.66215115	1.3664	11	0.00185

1

Perturbation coefficients and high order rotational constants ^(a)					
K ℓ'	Sym	P ₁	P ₂	P ₃	H x 10 ⁻¹¹ [cm ⁻¹]
-7	E _u	0.1760	9.6954	-1.3818	
-6	E _u				-240.7280
-4	E _u	2.8068	21.2584	-1.7843	338.1293
-3	G _s	0.2090	5.9299	-0.9862	
1	A _s				5.2861 ^(c)
1	E _s				51.1299 ^(c)
2	G _s	0.4384	23.9358	-1.0348	
3	E _s	0.3688	11.2986	-1.9035	
3	G _s	0.3524	13.5662	-1.7339	
7	A _u	0.0367	15.4387	-0.1476	
8	G _s	0.3183	20.7249	-1.3233	
10	A _s	0.0430	16.4071	-1.3051	
10	E _s	0.1812	17.6675	-0.9935	
Rotational constants for the -8 > K > 10 ^(d)					
ν ₀ = 2985.3953		B' = 0.66311490		Aζ' = 0.34385599	
A'-B' = 2.0208281		D _J '=8.9352 x 10 ⁻⁷		D _{JK} '= 6.8549 x 10 ⁻⁶	
D _K ' = -2.0192 x 10 ⁻⁵		n _J ' = -7.82 x 10 ⁻⁵		n _K ' = -7.12 x 10 ⁻⁴	
Intensity factors for the ν ₇ band of ethane					
S _v ⁰ (296K) = 301(24) [cm ⁻² atm ⁻¹] = 1.21(10) x 10 ⁻¹⁷ [cm ⁻¹ /(molecule cm ⁻²)]					
α = 0.0096(20)		β = -0.0034(20)		Q _R (296K)=51617	
Lineshape parameters for K beyond those reported in Malathy Devi et al. [2010a,b] ^(e)					
n ₁ (N ₂ temperature dependence): A = 0.6756 B = 0.0112 (J ₀ =0)					
n ₂ (SELF temperature dependence): A = 0.5687 B = 0.0085 (J ₀ =0)					
b _L ⁰ (N ₂) width:		a ₀ = 0.1011 a ₁ = -1.3352 x 10 ⁻³ a ₂ = 1.9690 x 10 ⁻⁵			
b _I ⁰ (SELF) width:		b ₀ = 0.1401 b ₁ = -1.6279 x 10 ⁻³ b ₂ = 2.3211 x 10 ⁻⁵			

2

3

4

5

6

7

8

9

10

11

12

13

Table 1: Spectroscopic constants for the ν_7 band of ethane. (a) Rotational constants and perturbations were obtained for each K -ladder considering equations 2 and 3. (b) For RQ_0 , limitations in the description of the ground-state were circumvented by defining a different set of upper-state rotational constants for $\Delta J \neq 0$. (c) Rotational constants for the RQ_0 ($\Delta J=0$) branch were obtained from Pine and Stone 1996. (d) For high K sub-bands, we fitted the energies of all lines (with the exception of the highly perturbed $K''=4,5,6$) to the global progression presented in equations 4 and 5. (e) For lines accessing K'' higher than those available in Malathy Devi et al. [2010a,b], we considered the mean progressions as presented in Figure 4.

1
2

Level	ℓ	K	J	D _{3d} notation	G ⁺ ₃₆ notation
Ground (A_{1g})	0	0	0,2,4	A _{1g} (8)	A _{1s} (6) + E _{3s} (2)
			1,3,5	A _{2g} (16)	A _{2s} (10) + E _{4s} (6)
		1,2,4,5 3,6,9	All	E _g (20)	E _{1s} (4) + G _s (16)
				A _{1g} (8)+A _{2g} (16)	A _{1s} (6) + E _{3s} (2) + A _{2s} (10) + E _{4s} (6)
ν_7 (E_u)	-1	0,1,3,4,6,7		E _u (20)	E _{2s} (4) + G _s (16)
		2,5,8		A _{1u} (8)+A _{2u} (16)	A _{3s} (6) + E _{3s} (2) + A _{4s} (10) + E _{4s} (6)
	+1	0,2,3,5,6,8		E _u (20)	E _{2s} (4) + G _s (16)
		1,4,7		A _{1u} (8)+A _{2u} (16)	A _{3s} (6) + E _{3s} (2) + A _{4s} (10) + E _{4s} (6)

3
4
5
6
7
8

Table 2: Symmetries of the rotational levels of the ground and ν_7 vibrational states considering the D_{3d} and G⁺₃₆ point groups. The G⁺₃₆ permutation-inversion group is used when internal torsional tunneling is considered. Statistical weights for each spin species are presented in brackets.

1

ID	Frequency [cm ⁻¹] ^(a)	E _{rot} [cm ⁻¹]	g-factor ^(c) x 10 ⁻⁵ [s ⁻¹]	Trans.	TOA Flux ^(b) x 10 ⁻¹⁸ [W m ⁻²]		Production rate x 10 ²⁶ [s ⁻¹]	
Comet C/2007 W1 (Boattini) – Trot = 79K							2.3513	0.0173
^R Q ₄	3000.2124	90.81	1.58545	0.8666	1.0369	0.0250	2.3613	0.0569
^R Q ₂	2993.4586	73.30	2.55965	0.9100	1.6418	0.0244	2.3210	0.0345
^R Q ₁	2990.0776	63.13	3.07130	0.8132	2.0151	0.0256	2.3770	0.0301
^R Q ₀	2986.7182	56.56	3.97371	0.9453	2.6096	0.0204	2.3818	0.0186
^P Q ₁	2983.3840	58.10	3.06727	0.9581	1.9262	0.0212	2.2802	0.0250
^P Q ₂	2980.0774	67.43	2.58050	0.7873	1.7046	0.0267	2.4011	0.0375
^P Q ₃	2976.7854	81.82	2.19640	0.9491	1.4041	0.0242	2.3263	0.0401
Comet C/2004 Q2 (Machholz) – Trot = 93K							13.309	0.2514
^R Q ₄	3000.2230	108.50	1.62755	0.8664	4.0881	0.0623	12.835	0.1955
^R Q ₂	2993.4579	84.47	2.44481	0.7769	6.1209	0.0719	12.822	0.1506
^R Q ₁	2990.0752	75.42	2.85883	0.7882	7.4671	0.0604	13.392	0.1082
^R Q ₀	2986.7144	69.13	3.65410	0.8820	10.148	0.0643	14.256	0.0903
^P Q ₁	2983.3840	69.34	2.84345	0.8796	7.1421	0.0498	12.907	0.0900
^P Q ₂	2980.0768	78.37	2.45732	0.7311	6.3405	0.1423	13.274	0.2979
^P Q ₃	2976.7883	93.62	2.18030	0.9213	5.3157	0.0585	12.556	0.1381
Comet 8P/Tuttle – Trot = 60K							1.7383	0.0594
^R Q ₄	3000.2855	100.18	0.95049	0.9095	0.2265	0.0406	1.6573	0.2969
^R Q ₁	2990.0819	49.10	3.29522	0.7555	0.8215	0.0686	1.7396	0.1452
^R Q ₀	2986.7192	42.09	4.48408	0.8769	1.1869	0.0468	1.8490	0.0729
^P Q ₁	2983.3820	44.73	3.36980	0.9115	0.7589	0.0425	1.5749	0.0882
^P Q ₂	2980.0731	51.61	2.69160	0.7414	0.6785	0.0624	1.7649	0.1622

2

3 **Table 3:** IDs, frequencies (ν), weighted rotational energies (E_{rot}), TOA g-factors (g) at
4 $R_h=1\text{AU}$, transmittances, TOA measured fluxes and production rates (Q) for 7 Q sub-
5 branches of the ν_7 band of C_2H_6 . a) The rest-frequency is the weighted mean of the
6 frequencies composing each Q-branch, where the weight is the g-factor x transmittance
7 for each compounding line. b) Total transmittance-corrected flux considering a $0.432 \times$
8 1.782 arcsec^2 box for the W1 and Q2 results (NIRSPEC) and $0.400 \times 1.29 \text{ arcsec}^2$ for the
9 8P results (CRIRES). c) Integrated fluorescence efficiencies in the spectral region of the
10 corresponding Q-branch from the new model synthesized with the appropriate rotational
11 temperatures and heliocentric velocities – 8P/Tuttle: $T_{\text{rot}} = 60 \text{ K}$ and $v_h = -0.37 \text{ km s}^{-1}$,
12 C/2007 W1: $T_{\text{rot}} = 79 \text{ K}$ and $v_h = +9.70 \text{ km s}^{-1}$, C/2004 Q2: $T_{\text{rot}} = 93\text{K}$ and
13 $v_h = -2.01 \text{ km s}^{-1}$.

14

1

Atmosphere	1. Abundance relative to std. profile	2. Ethane (C ₂ H ₆) Mixing ratios
Mars – Ethane (C₂H₆) search ^(a)		
62°N-62°S, 295-308°W at L _s =323° (MY 29), 18 August 2009		< 0.8 ppb (3σ)
41°N-76°S, 57-67°W at L _s =352° (MY 27), 6 January 2006		< 1.5 ppb (3σ)
Earth – Ethane (C₂H₆) surface level volume mixing ratio ^(b)		
Mauna Kea (4,200 m, Hawaii), 6 Jan 2006	0.49 ± 0.03	(0.97 ± 0.06) ppb
Paranal (2,635 m, Chile), 18 August 2009	0.15 ± 0.02	(0.30 ± 0.04) ppb
Comets - Ethane (C₂H₆) abundance relative to water (H₂O) ^(c)		
C/2007 W1 (Boattini), 9 July 2008, NIRSPEC at Keck II		(1.957 ± 0.053) %
C/2004 Q2 (Machholz), 19 January 2005, NIRSPEC at Keck II		(0.488 ± 0.016) %
8P/Tuttle , 26 January 2008, CRIRES at VLT		(0.291 ± 0.017) %

2

3 **Table 4:** Measured ethane abundance in selected planetary and cometary atmospheres. **a)**
4 Mars: We searched for ethane at 7 latitudinal intervals along the central meridian in
5 August 2009 and January 2006, achieving extremely high sensitivities. The spectra
6 presented in Figs. 4 and 5 also sample the methane P-branch, allowing us to obtain in Jan
7 2006 a sensitive upper limit for CH₄ of < 8 ppb [3σ] (consistent with Mumma et al.
8 2009). The data taken with CRIRES in August 2009 were test exposures and the
9 Doppler-shift (-9.4 km s⁻¹) was not sufficient to search for CH₄ on Mars. **b)** Assuming
10 the “standard” Northern hemisphere vertical profile as presented in Fig 3c, we retrieved
11 the scaling factor presented in column ‘1’. A value of 0.15 (1/7) is consistent with the
12 findings of Helmig et al. 2009 for the Southern Hemisphere. Mixing ratios at surface
13 level on site are presented in column ‘2’. The value for Mauna Kea is similar to the
14 findings of Rinsland et al. [1994] for Mauna Loa at this season (corrected for hot-band
15 absorption, see text). **c)** The ethane mixing ratios in comets are defined with respect to
16 water, the main volatile constituent.

17

18

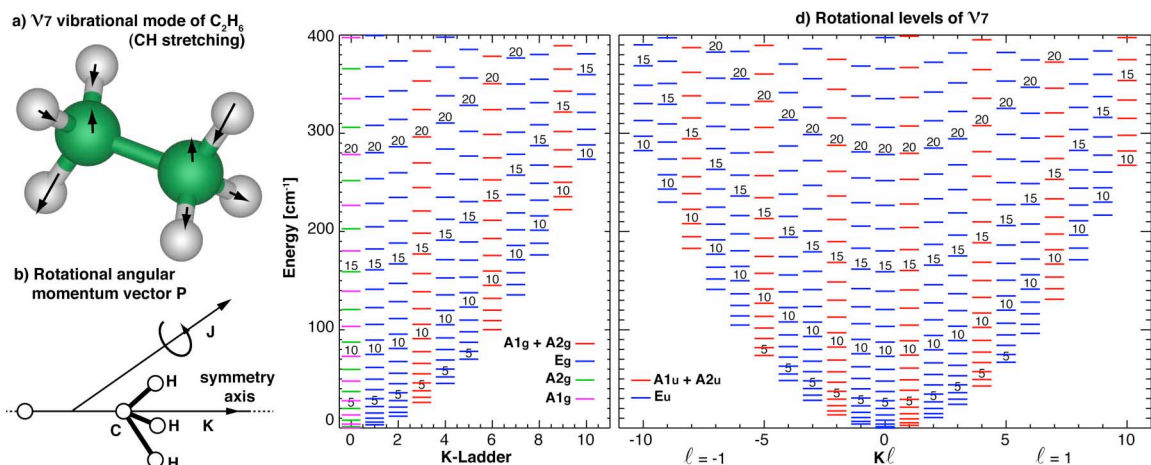


Figure 1. Rotational structure of the ground and ν_7 vibrational levels of C_2H_6 . Panel ‘a’ shows the relative motions of the atoms of C_2H_6 associated with the ν_7 vibrational mode. Panel ‘b’ shows the rotational angular momentum (related to the J quantum number), and its projection along the symmetry-axis (related to the K quantum number). Panels ‘c’ and ‘d’ show rotational levels for the ground and ν_7 vibrational states, respectively, with symmetries indicated by different trace types.

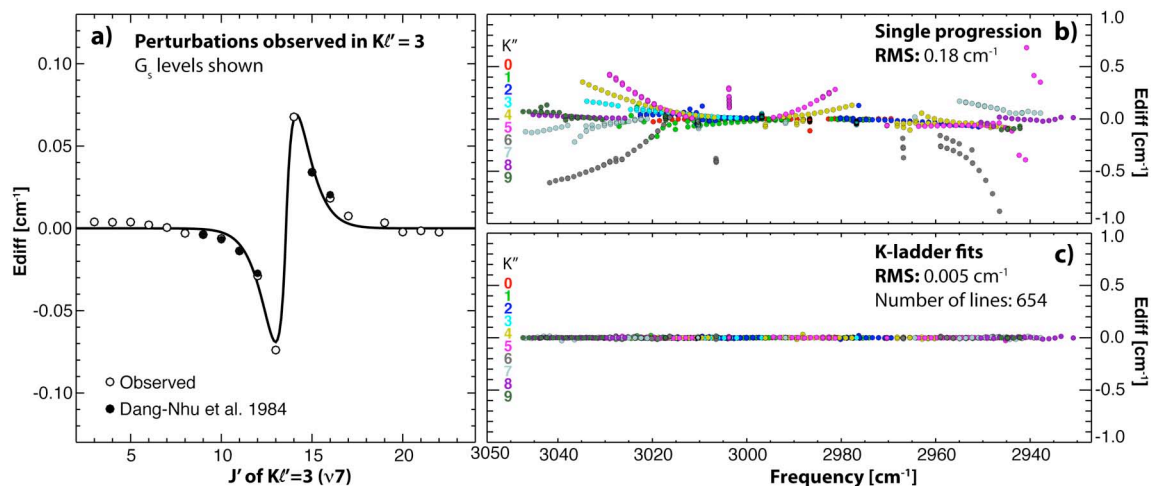


Figure 2: Description of the rotational levels of the ν_7 vibrational state. Panel ‘a’ shows the effect of local perturbations on the energy distribution of the rotational levels. The empirical values were fitted to a quadratic progression and a perturbation function (trace) considering the values presented in Table 1. Panel ‘b’ shows the energy residuals obtained when performing a global fit to the rotational lines of the ν_7 vibrational level using a single progression for all K -ladders. Panel ‘c’ shows the residuals for 654 lines using individual coefficients for each K -ladder (see Table 1).

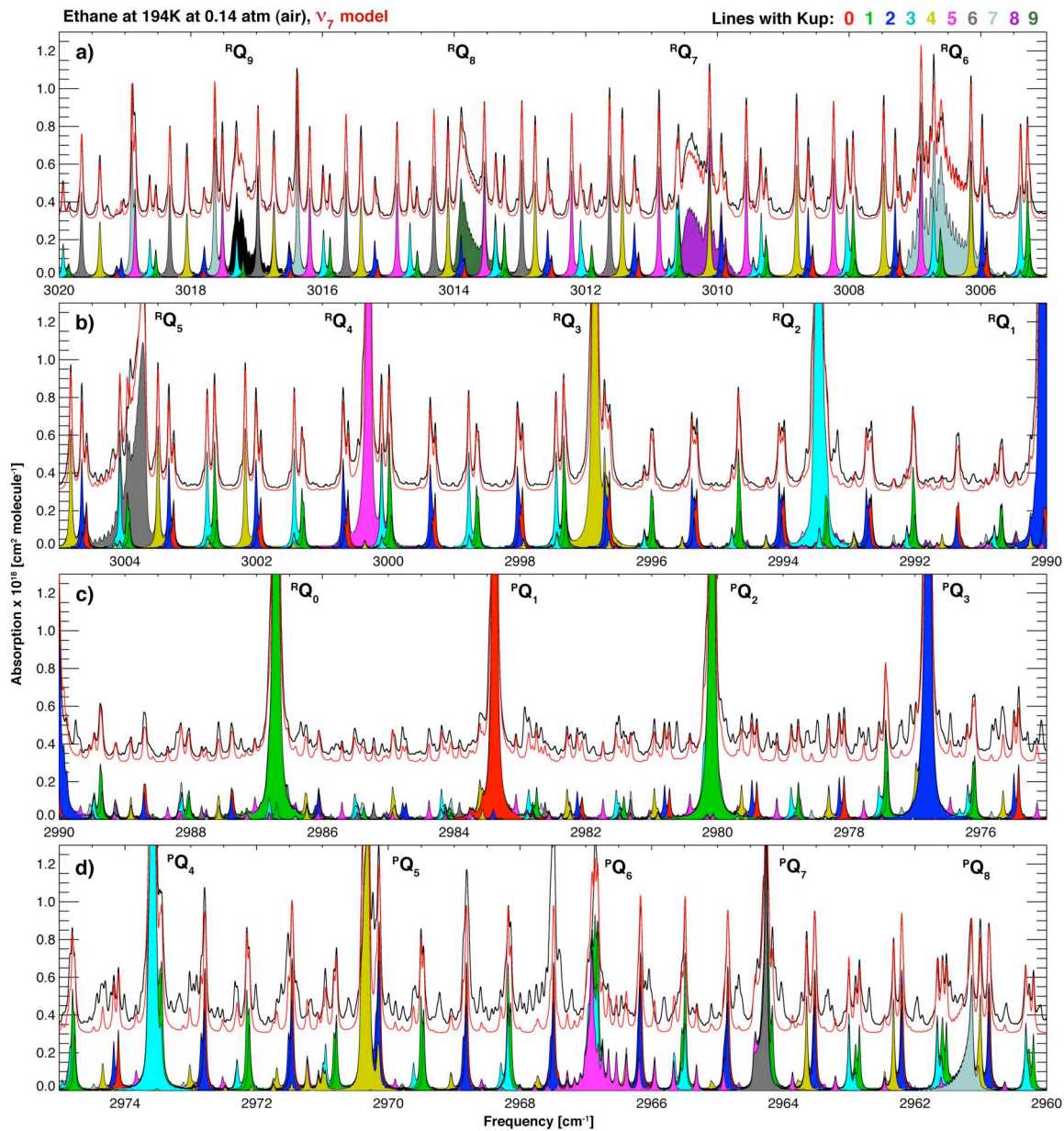


Figure 3: Individual K sub-bands of the ν_7 band of ethane compared to absorption cross sections obtained by Harrison et al. [2010] for a temperature of 194K and a pressure of 0.14 atm of synthetic air. The total model (red) and measured (black trace) absorption cross sections have been displaced by 0.3 for clarity purposes.

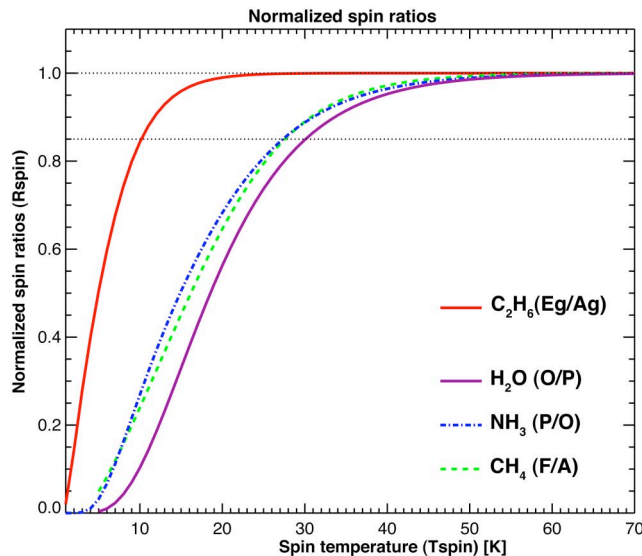


Figure 4: Symmetry ratio of ethane ($A_g = A_{1g} + A_{2g}$ and E_g considering the D_{3d} point group, $E_g/A_g=5/3$ at equilibrium) in comparison to water (H_2O , $O/P=3$ at eq.), ammonia (NH_3 , $P/O=1$ at eq.) and methane (CH_4 , $F/A=9/5$ at eq.).

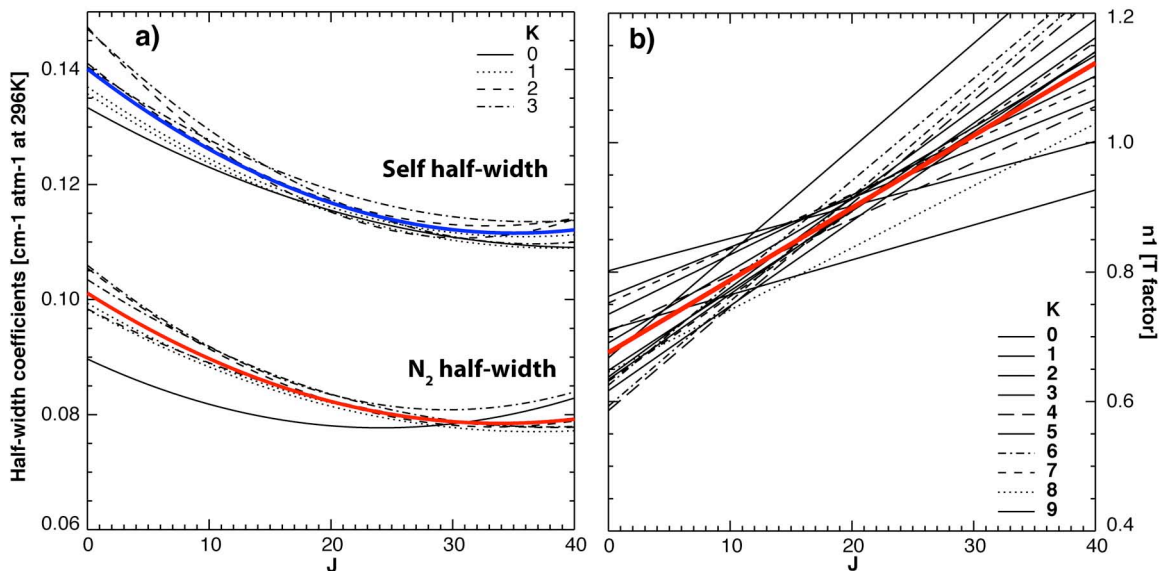


Figure 5: Lineshape parameters progressions retrieved by Malathy Devi et al. [2010a,b] for the ν_9 band of ethane and applied to our model of the ν_7 band. For K values with no available measurements we computed a weighted mean progression, shown in the figure with a thick color trace. The coefficients of the weighted mean progressions are presented in Table 1.

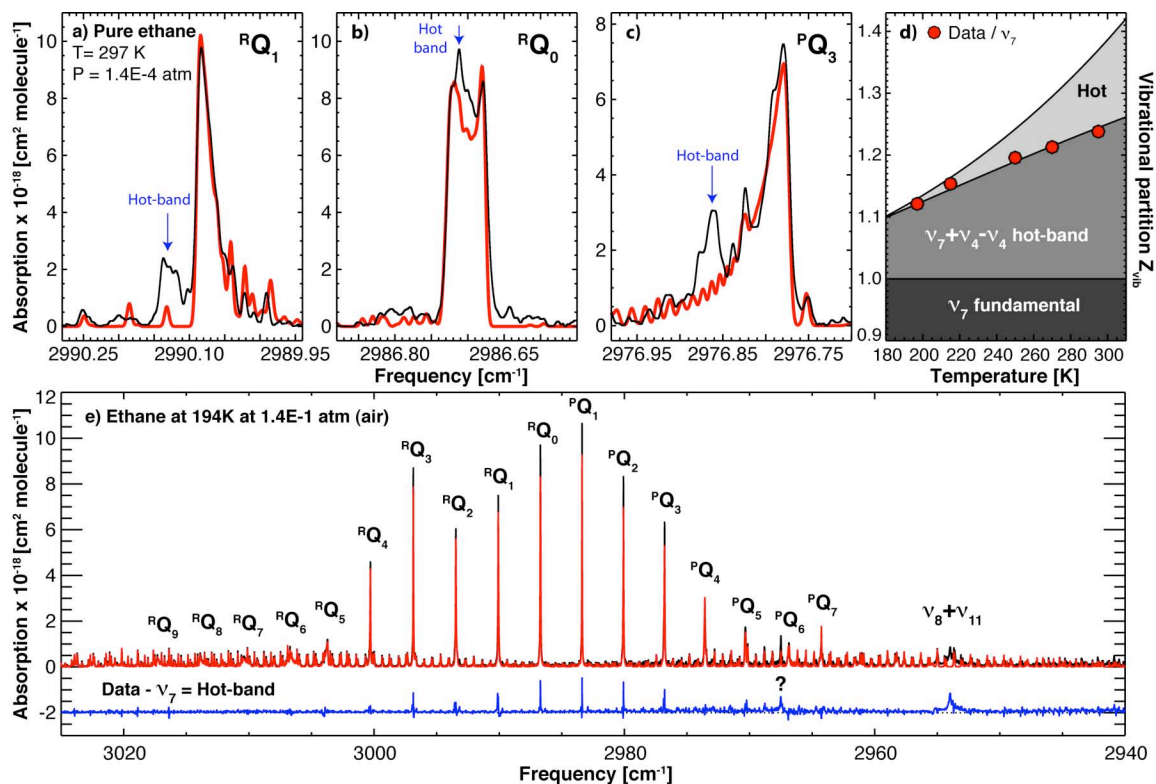


Figure 6: Identification of the ν_7 hot-band of ethane. Panels ‘a’, ‘b’ and ‘c’ show comparisons of model spectra with pure ethane spectra recorded by Harrison et al. [2010] at 297K and 1.4×10^{-4} atmospheres. At these low pressures, the fine structure of the Q-branches is nicely revealed, showing unaccounted absorptions that we associate with the first torsional hot-band of the ν_7 band. Panel ‘d’ shows the ratio of the area of the strongest Q-branches ($K'' \leq 4$, with the exception of PQ_1 , see text) with respect to the modeled ν_7 absorption, integrated around ($\pm 0.3 \text{ cm}^{-1}$) at each K-band center. The fact that the ratio coincides with the vibrational partition function of the ν_7 level and its first torsional component suggests that these absorptions are related to the $\nu_7 + \nu_4 - \nu_4$ hot-band.

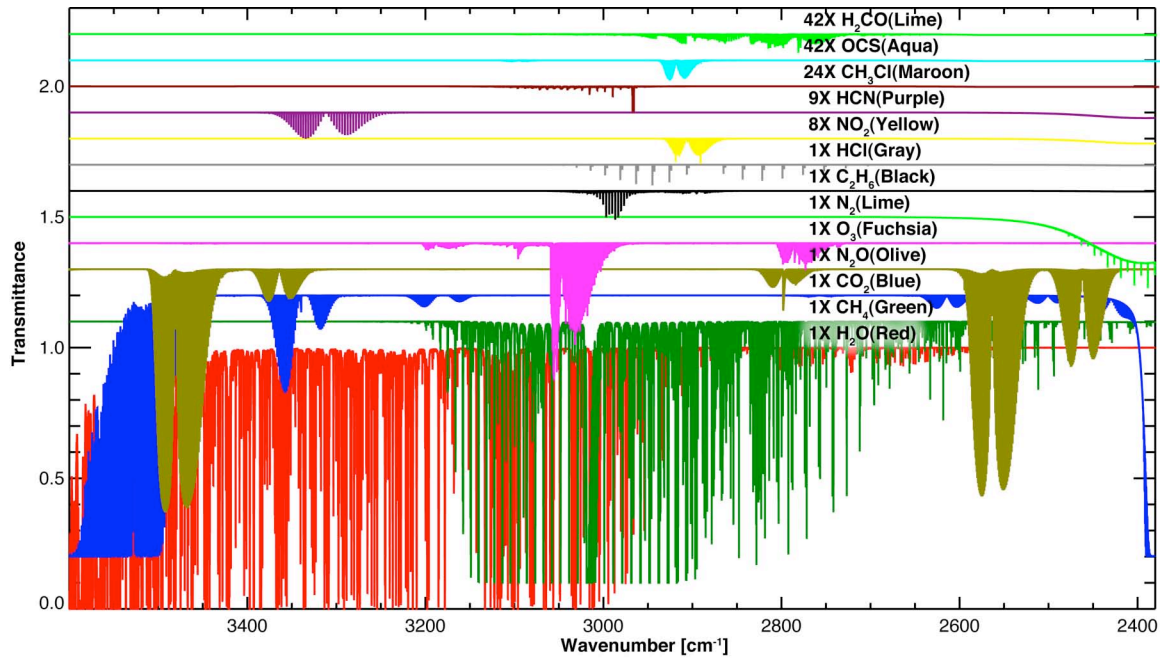


Figure 7. Representative terrestrial spectra synthesized with the LBLRTM line-by-line and layer-by-layer radiative transfer model, and utilizing our updated spectral database. The spectra were synthesized for airmass 1.0 (zenith), and (adopted) nominal abundances, temperatures and pressures for Mauna Kea at 4,200 m altitude.

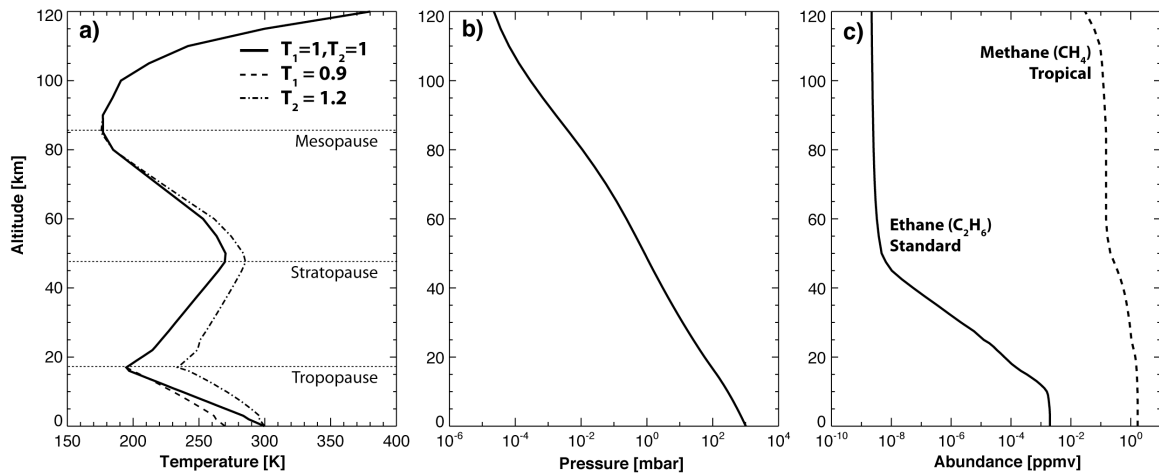


Figure 8. Vertical profiles of temperature (a), pressure (b), and mixing ratios for CH_4 and C_2H_6 (c) adopted for synthesizing terrestrial spectra. The temperature profile ‘a’ is organized into tropospheric (affected by T_1) and stratospheric (affected by T_2) sectors, while the pressure profile (Panel ‘b’) is the standard tropical pressure profile scaled with a multiplier (see text). Temperatures and pressures are scaled relative to the standard tropical value (Anderson et al. 1986).

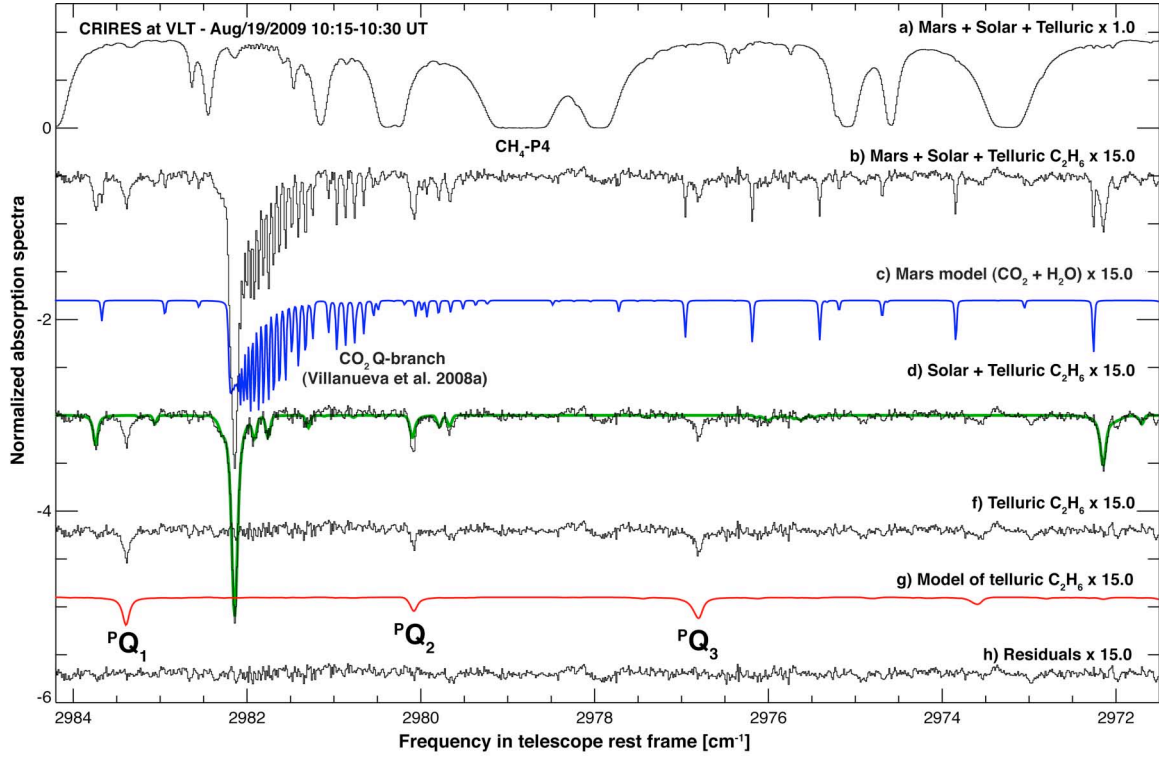


Figure 9. Mars infrared spectrum taken on 18 August 2009 with CRIRES at VLT (total of 8 minutes integration time on source). Trace ‘a’ shows the calibrated Mars continuum affected by terrestrial transmittance, and trace ‘b’ shows the Mars residual spectrum after removing a terrestrial model (with no C₂H₆). Trace ‘d’ shows the residual spectrum after removing a Martian absorption spectrum containing CO₂ and H₂O (trace ‘c’). Trace ‘d’ shows the residual spectrum containing solar Fraunhofer lines and telluric C₂H₆ lines, while trace ‘e’ is a model of the solar spectrum considering the new method presented in Appendix B. Trace ‘f’ shows the residual telluric ethane spectrum, and trace ‘h’ shows the overall residual after removing a terrestrial spectrum synthesized with the new C₂H₆ v₇ band model (trace ‘g’).

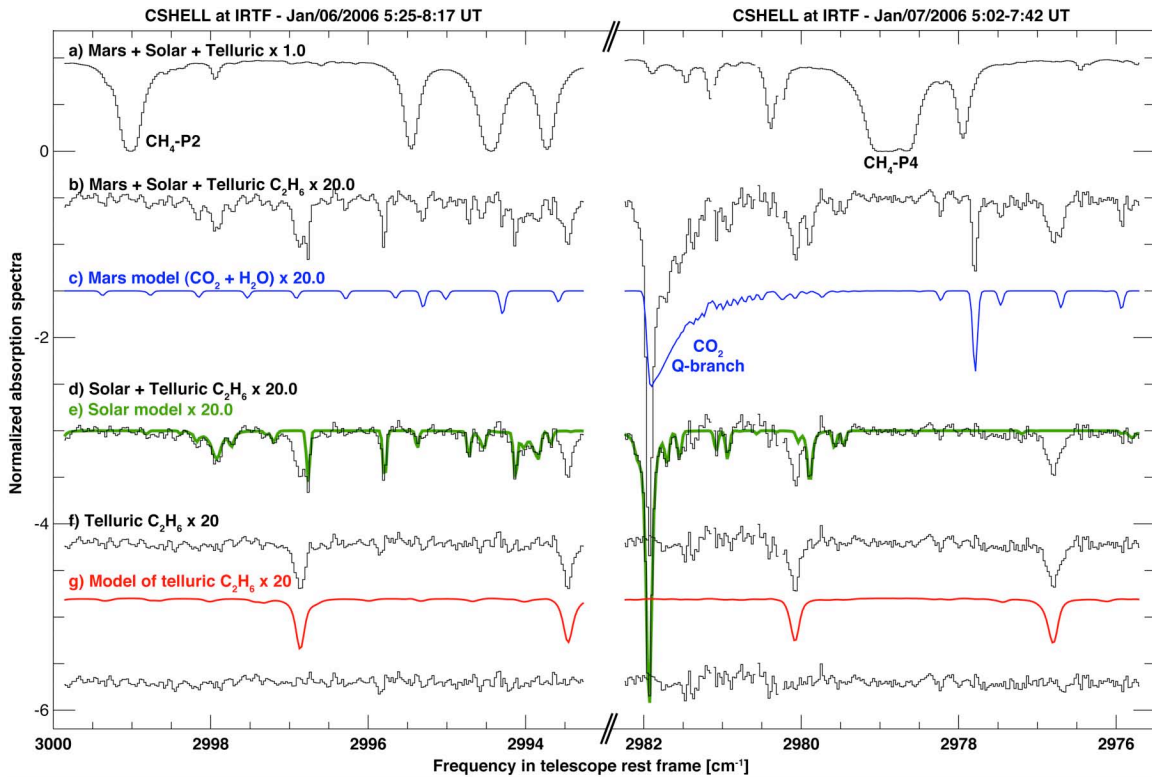


Figure 10. Mars infrared spectra taken on 6-7 January 2006 using two CSHELL-IRTF settings (the total integration time on source was 40 (52) minutes for the left (right) spectrum). See Figure 4 for a description of the traces. The spectral sharpness of the spectral features is higher in Figure 4 because of higher resolving power ($\lambda/\Delta\lambda \sim 90,000$) with CRISP (for CSHELL, $\lambda/\Delta\lambda \sim 40,000$). The terrestrial C_2H_6 lines appear stronger in the Northern hemisphere (compare Southern Hemisphere, Figure 4) because of the higher abundance of volatile organic compounds (VOCs, including C_2H_6) that arise mainly from biogenic and anthropogenic emissions.

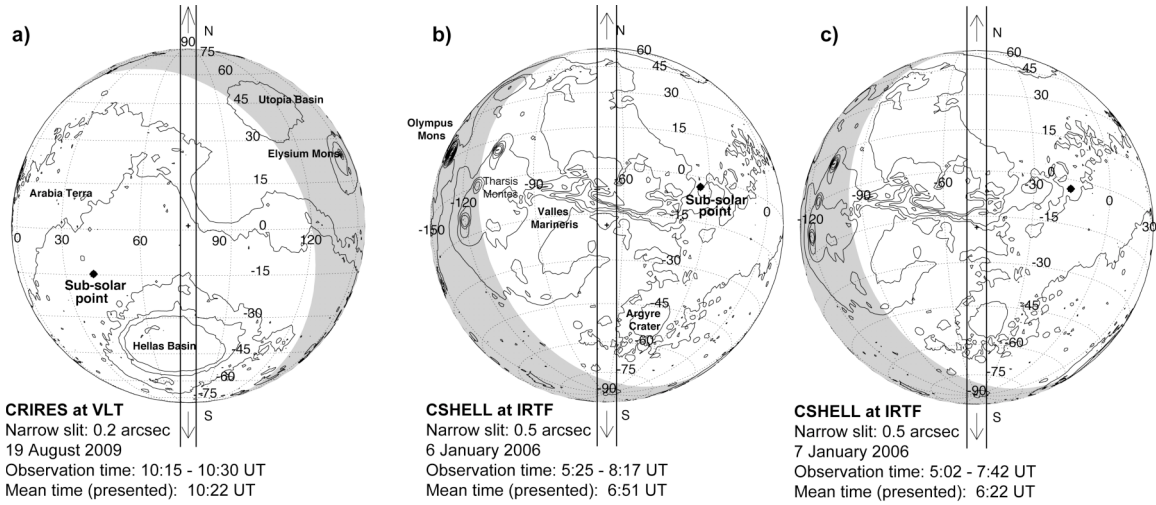


Figure 11. Geometry diagrams presenting the orientation of the spectrometer's entrance slit for CRIRES data taken on 19 August 2009 (a), and CSHELL data taken on 6-7 January 2006 (b and c panels). We used the narrowest slit for each instrument (0.2'' for CRIRES, 0.5'' for CSHELL), and oriented the slit North-South on the planet for the three measurements.

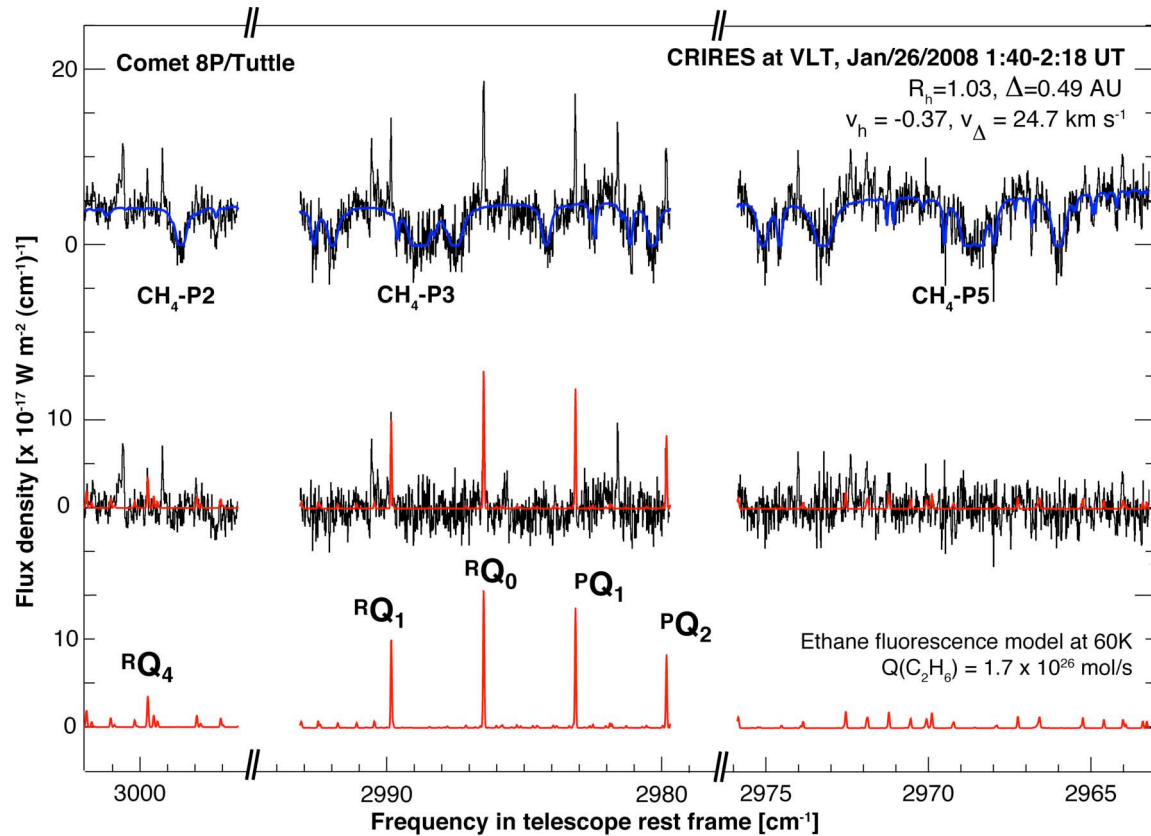


Figure 12. Infrared spectrum of comet 8P/Tuttle taken on 26 January 2008 using CRIRES at VLT (Bönnhardt et al. 2008). The upper trace shows a spectrum extracted from the sum of 15 spatial rows centered on the comet nucleus, and a continuum model affected by terrestrial transmittance is overlaid. The mid-trace (residual spectrum) reveals lines of the ν_7 band of C_2H_6 in emission (with model overlaid).

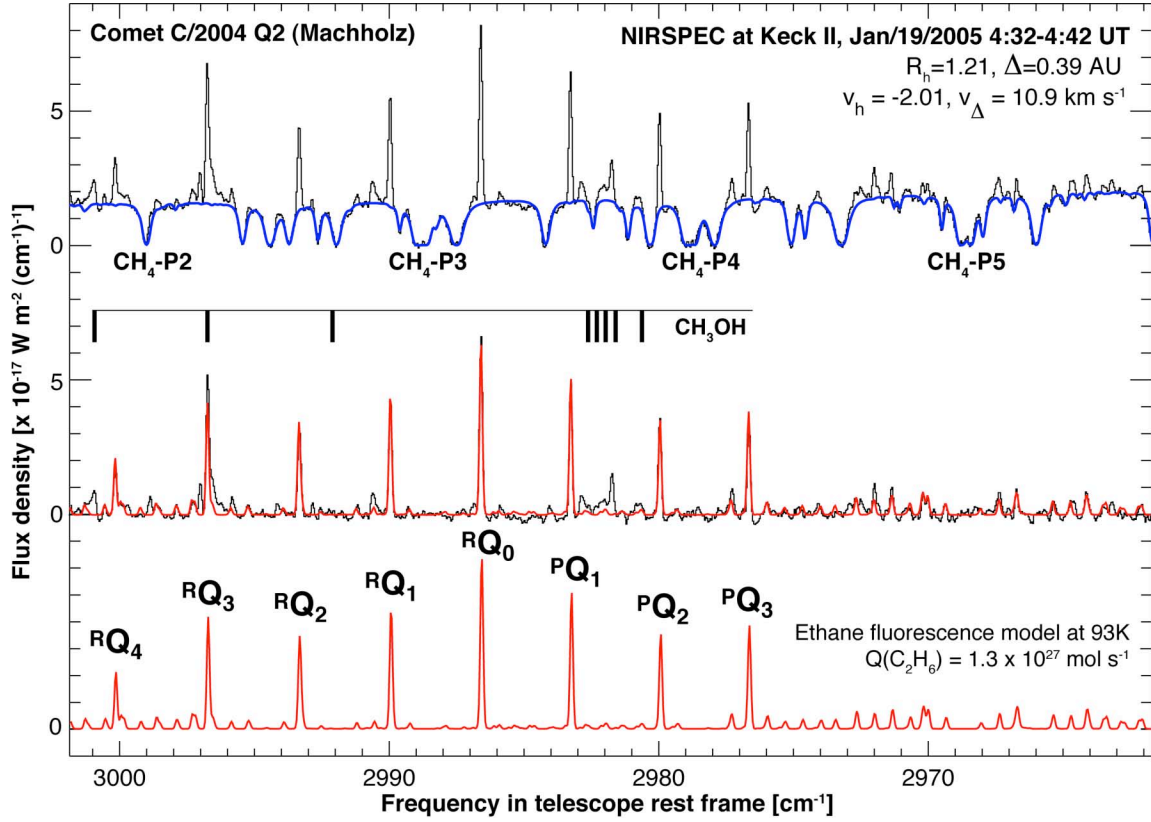


Figure 13. Infrared spectrum of comet C/2004 Q2 (Machholz) taken on 19 January 2005 using NIRSPEC at Keck II (Bonev et al. 2009). The upper trace shows the measured spectrum extracted from the sum of 9 spatial rows centered on the comet nucleus, and a continuum model affected by terrestrial transmittance is overlaid. The mid-trace shows the emission residual that reveals the ν_7 band of C_2H_6 (with model overlaid) and certain CH_3OH lines.

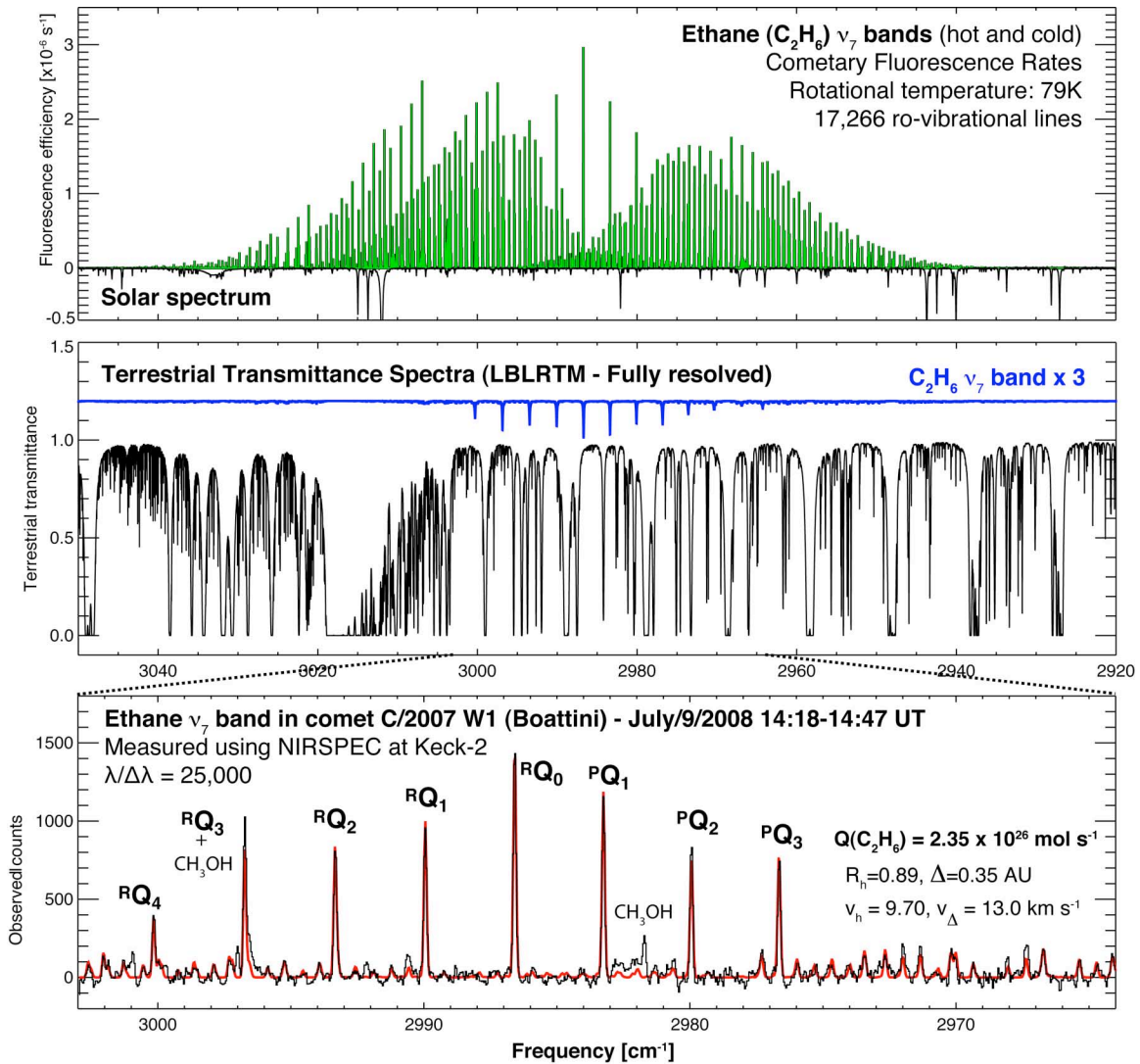


Figure 14. Fluorescence model of the ν_7 bands of C_2H_6 and comparison with spectra of comet C/2007 W1 (Boattini) taken on 10 July 2008 with NIRSPEC at Keck II. **Upper-panel:** ethane fluorescence emission rates (g-factors) for 17,266 lines of ν_7 (fundamental band) and $\nu_7 + \nu_4 - \nu_4$ (hot-band) with $T_{rot} = 79 \text{ K}$, $v_h = +9.70 \text{ km s}^{-1}$ and $R_h = 1 \text{ AU}$. **Mid-panel:** terrestrial transmittance and telluric C_2H_6 absorption synthesized using LBLRTM. **Lower-panel:** High-resolution spectrum of comet Boattini showing the fine structure of the ν_7 band of C_2H_6 (with model overlaid) and certain CH_3OH lines.

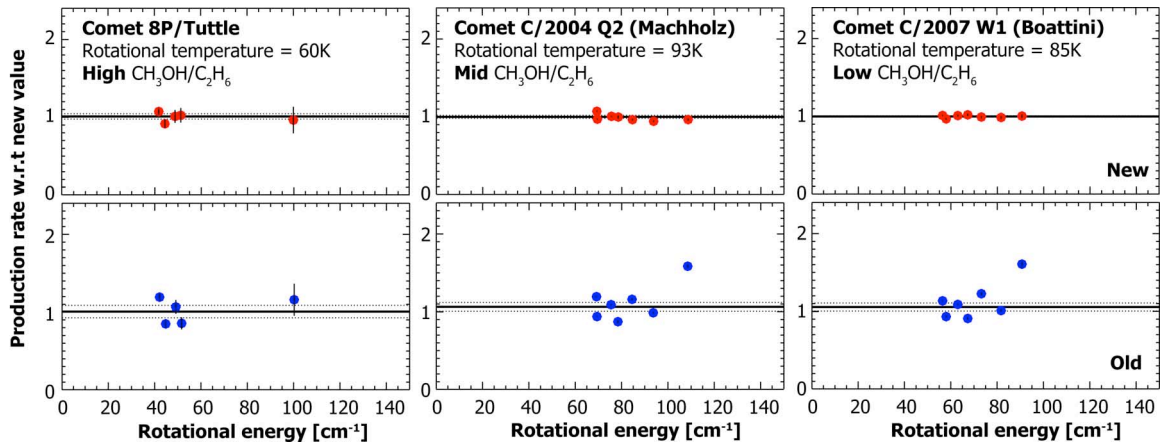


Figure 15. Excitation diagrams showing total production rates retrieved from individual ethane Q sub-branches, based on the new and old models (see details in Table 1). Results considering the new model are shown relative to the “new” mean in the upper panels, while the “old” results are presented in the lower panels.

Appendix A: HITRAN corrections and updates

We use the universally recognized HITRAN database as the base for our radiative transfer model (using LBLRTM) and include our own corrections and updates. To the HITRAN 2008 release: 1) we applied the current updates available on the HITRAN website (<http://www.cfa.harvard.edu/hitran/updates.html>); 2) we added our new model for the ν_7 and $\nu_7+\nu_4-\nu_4$ bands of C_2H_6 (17,266 spectral lines); and 3) we expanded the CO_2 database to include our latest discoveries in the Martian atmosphere (1780 lines of 4 bands, see below).

We recently discovered multiple unknown isotopic bands of CO_2 not previously described in the refereed literature (and not present in the HITRAN atlas), when analyzing spectra of CO_2 -rich Mars [Villanueva et al. 2008a,b]. The observations were performed using high-resolution echelle spectrometers, allowing us to extract precise spectroscopic constants for the levels involved (see Table 1 of Villanueva et al. [2008b] for the $\nu_2 + \nu_3$ band of $^{16}\text{O}^{12}\text{C}^{18}\text{O}$ at 3.3 μm , the $2\nu_1$ band of $^{16}\text{O}^{12}\text{C}^{17}\text{O}$ at 3.6 μm , and the $2\nu_1$ band of the rare isotope $^{16}\text{O}^{13}\text{C}^{18}\text{O}$ at 3.7 μm). In a follow-up study by the Venus Express SOIR Team, our detection of $2\nu_1$ ($^{16}\text{O}^{13}\text{C}^{18}\text{O}$) band was confirmed and they have recently retrieved an improved set of spectroscopic constants for this band [Vandaele et al. 2009]. A compilation of all constants is presented in Table A-1.

1

Level	G_v [cm ⁻¹]	B_v [cm ⁻¹]	D_v [cm ⁻¹] x10 ⁻⁷	H_v [cm ⁻¹] x10 ⁻¹³	S_v^0 [cm ⁻¹ / mol cm ⁻²] x10 ⁻²⁵	a1
¹⁶O¹²C¹⁸O (CO₂ 628) – Villanueva et al. 2008a, Rothman et al. 1992						
00001	0.0	0.36818450	1.18647	-0.150		
01111e	2982.11105	0.36573112	1.20268	0.217	1.83	-0.003
01111f		0.36626757	1.20380*	-0.296*		
¹⁶O¹²C¹⁷O (CO₂ 627) – Villanueva et al. 2008b, Rothman et al. 1992						
00001	0.0	0.37861462	1.26428	0.000		
20001	2775.58690	0.37931621	1.48387	0.000	2.14	
¹⁶O¹³C¹⁸O (CO₂ 638) – Villanueva et al. 2008b, Vandaele et al. 2009, Rothman et al. 1992						
00001	0.0	0.36818116	1.18498	0.000		
20001	2701.932484	0.36833043	0.872951	0.000	0.53	

2

3

4

5

6

Table A-1. Carbon dioxide (CO₂) ro-vibrational constants and band strengths. The band strengths are for transitions from the ground level and for an excitation temperature of 296K. The value ‘a1’ is the first Herman-Wallis coefficient (Eq. 14 in Rothman et al. 1992).

7

8

1 **Appendix B: Solar Spectrum**

2 We created a high-resolution flux-calibrated solar spectrum by combining an empirical
3 line-by-line model for the infrared solar transmittance [Hase et al. 2006] with a purely
4 theoretical model for the solar continuum irradiance [Kurucz 1997]; see Fig. B-1.
5 Knowledge of the solar spectrum has greatly improved in the last few decades, due to
6 spacecraft measurements (ATMOS mission [Abrams et al. 1996], ACE instrument [Hase
7 et al. 2010]), and the comprehensive solar survey performed at the McMath-Pierce
8 telescope at the Kitt-Peak National Observatory [Wallace and Livingston 2003]. These
9 measurements integrated light from the entire Solar disk, and thus include factors such as
10 limb darkening and other effects. One of the biggest limitations of these databases is that
11 they are not flux calibrated, and the spectra can only be used to extract transmittance
12 information. On the other hand, theoretical models have been extremely successful in
13 calculating a flux-calibrated solar continuum, but their prediction of solar spectral
14 features is still not optimum. There are several theoretical solar models (e.g. [Tobiska et
15 al. 2000]). The Kurucz [1997] solar irradiance spectrum is considered best when
16 averaged to [nm] resolutions [Fiorenza and Formisano 2005], but it does not describe the
17 spectral morphology precisely (See Fig. B-2). In the case of the flux-calibrated solar
18 spectrum presented in Fiorenza and Formisano [2005], we could not reproduce their
19 reported values, and we suspect of an incorrect labeling of their flux units.

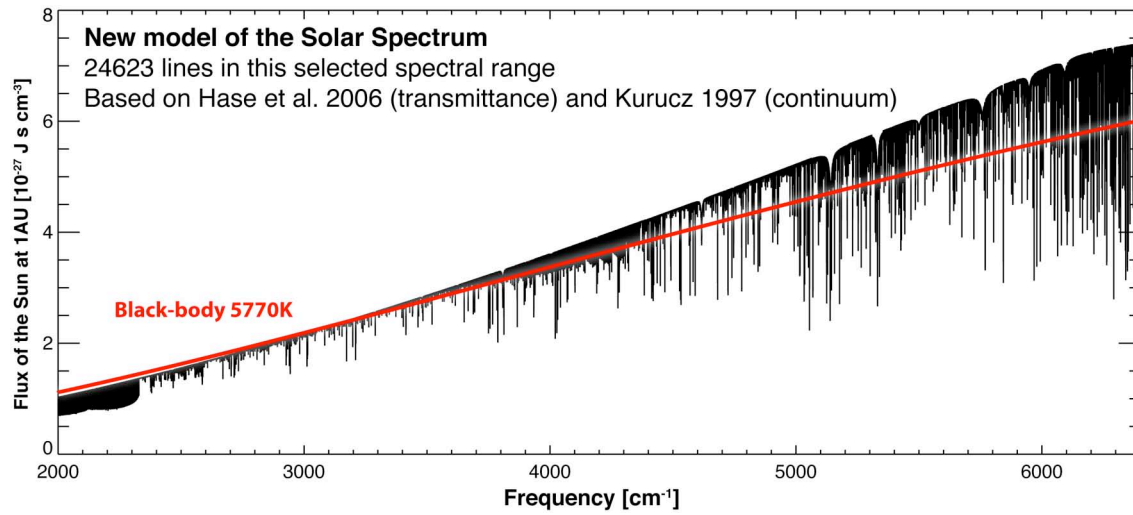
20 Using the ATMOS spectrum and other ground-based measurements of the Sun, Hase et
21 al. [2006] generated an empirical line-by-line list model of the solar transmittance
22 spectrum. Recently, the same group has constructed a highly sensitive infrared solar

1 spectrum from ACE-FTS observations [Hase et al. 2010] and they were able to assign
2 numerous weak absorption features (that were not detectable in the ATMOS solar
3 observations) due to the improved signal-to-noise of the ACE-FTS data. However, Hase
4 et al. [2010] did not create line-by-line empirical data, only solar transmittance as a
5 function of frequency.

6 The solar line list of Hase et al. [2006] includes intensities and identifications for each
7 line and a parameterization of the lineshape (Gaussian $w=0$, Lorentzian $w=1$). It also
8 accounts for center-to-limb variation of lines and continuum brightness temperature. In
9 addition, the synthetic spectrum generated in this manner has a much greater signal-to-
10 noise ratio, since each line can be properly described by just 4 line parameters. By
11 multiplying this realistic transmittance spectrum of Hase et al. [2006] with the highly
12 accurate continuum model of Kurucz [1997], we generated a flux-calibrated solar
13 spectrum in the wavelength range $700\text{-}6400\text{ cm}^{-1}$ (see Fig. 7). We simulate the integrated
14 disk-spectrum by convolving the synthetic spectra with a solar rotation line-profile,
15 which includes differential rotation (A:14.713 deg/day, B:-2.396 deg/day, C: -1.787
16 deg/day; Snodgrass and Ulrich, 1990), limb darkening ($u=0.6$) and the capability to
17 compute integrated disk spectra for different inclinations (see Fig. B-3). At the ecliptic
18 the broadening by this effect is $\sim 2.5\text{ km s}^{-1}$ (FWHM). This approximation is far from
19 optimum, but it provides an intermediate solution until a line-list for the integrated-disk at
20 different inclinations becomes available. This spectrum was used to compute the
21 fluorescence pumping in Eq. C-3. In Figure B-2 we show a comparison between the
22 spacecraft solar spectrum measured by the ATMOS instrument [Abrams et al. 1996], the
23 empirical line-by-line solar model using ATMOS data [Hase et al. 2006], the solar

1 spectrum of Hase et al. [2010] using ACE-FTS data, and the theoretical solar irradiance
2 spectrum by Kurucz [1997].

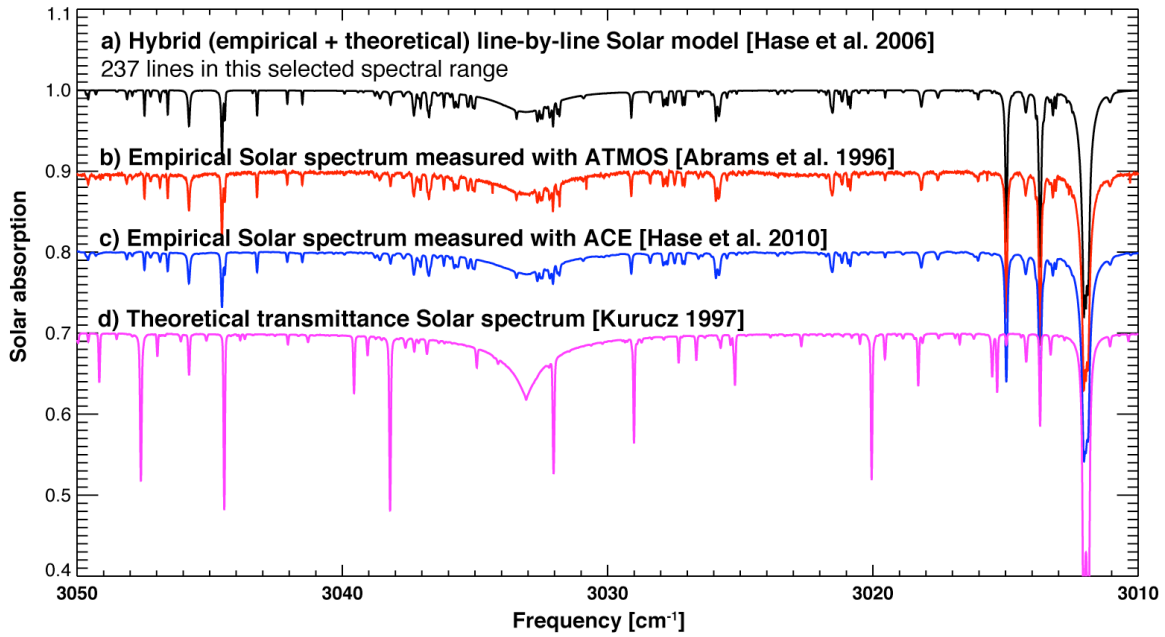
3



4

5 **Figure B-1.** Spectrum of the Sun in the near-infrared region (1.6 to 5 μm) based on a
6 theoretical model for the continuum [Kurucz 1997] and a new solar line list [Hase et al.
7 2006]. The grey trace shows the continuum of a black body at 5770 K.
8

1



2

Figure B-2. Comparison of measured and synthetic solar spectra. Trace 'a' was synthesized adopting 237 solar lines listed in the Hase et al. [2006] atlas and utilizing 4 parameters per line (center, strength, width and shape parameter). Trace 'b' is the solar spectrum as measured with the ATMOS instrument from the Space Shuttle, while 'c' is the solar spectrum as measured with the ACE instrument onboard SCISAT-1. Trace 'c' is the spectrum modeled by Kurucz [1997], with spectral lines included; it clearly does not reproduce the observed spectra (b, c). For clarity purposes, trace 'b' was shifted vertically by -0.1, trace 'c' by -0.2 and trace 'd' by -0.3.

11

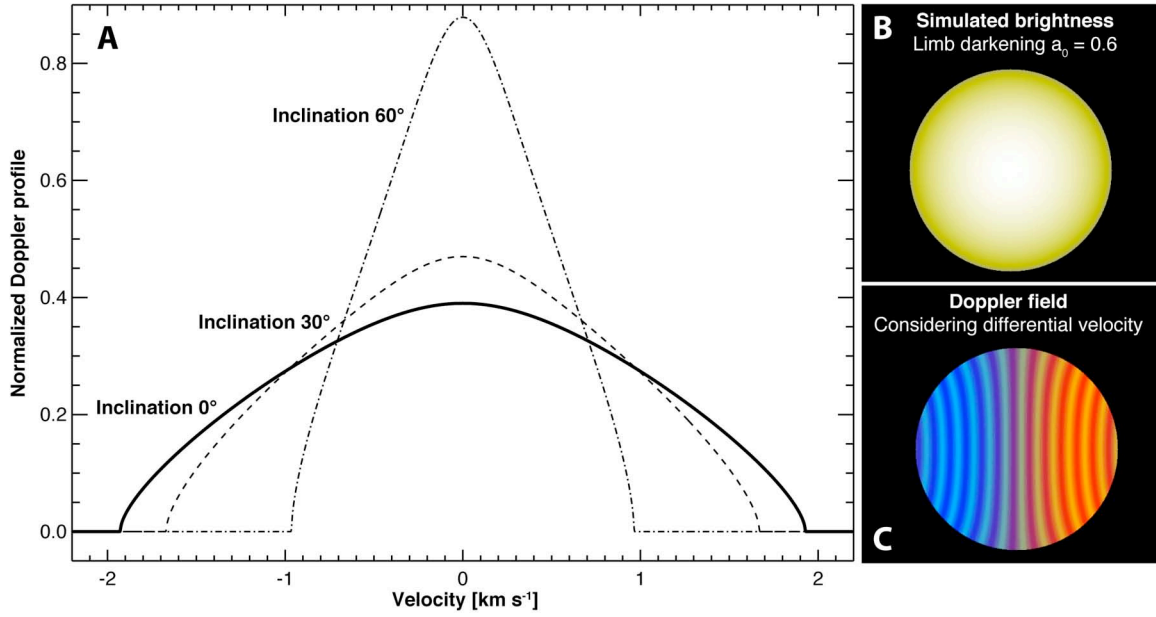


Figure B-3. **A.** Considered solar rotation Doppler profiles for different inclinations relative to the rotation plane. These profiles are used to transform the synthetic disk-center spectra by Hase et al. [2006] to disk-integrated spectra at different inclinations in the solar system. **B.** Simulated line intensity considered a limb darkening coefficient a_0 of 0.6. **C.** Doppler field computed considering latitude differential velocity using coefficients retrieved from Doppler measurements [Snodgrass and Ulrich, 1990]. Blue colors indicate motion towards the observer, while red colors indicate motions away from the observer. Yellow vertical lines are traces of iso-velocity.

Appendix C: General Fluorescence Model (GFM)

We require 11 parameters from the HITRAN database to compute g-factors: molecular identification (M), isotopologue number (I), frequency of the transition (ν [cm^{-1}]), Einstein A-coefficient (A_{21} [s^{-1}]), lower state energy (E'' [cm^{-1}]), upper and lower global vibrational quantum numbers (V' , V''), upper and lower local rotational quantum numbers (L' , L''), and upper and lower statistical weights (w' , w''). (To avoid confusing fluorescence emission rates (g-factors) with statistical weights, we use the letter 'w' (instead of the standard terminology, 'g') to refer to the latter). Even though Einstein A-coefficients can be computed from absorption line intensities [Šimečková et al. 2006], the inclusion of A-coefficients in HITRAN since 2004 (which replaced the weighted square of the transition moment) has been a great advance, and is of significant value to studies related to non-LTE processes.

In computing line-by-line fluorescence efficiencies (g-factors) we need to build a full quantum mechanical model for a molecular band. We illustrate that process for C_2H_6 . In the following sections we present how we (a) create the ro-vibrational structure of the energy levels, (b) compute the total partition function (Q_{tot}), (c) calculate pumping rates, and (d) calculate emission rates.

C.1. Re-creation of the ro-vibrational energy-levels

The ro-vibrational structure of the energy levels involved in a particular band system can be straightforwardly retrieved from the information of the individual lines in the HITRAN database (however, it is important to validate the numbers because numerous

1 errors exist in the database). For example, by isolating lines from a defined band, and
 2 using 6 parameters (ν , E'' , L' , L'' , w' , w'') for each line, we can recreate an indexed
 3 rotational structure (energy) of the lower and upper states: $E''(L'') = E_i''$; $E'(L') = E_i'' +$
 4 ν ; where i is the line index, and L' and L'' refer to the local quantum numbers for the
 5 levels that is determined by the rotational structure. For linear molecules like CO (carbon
 6 monoxide) and C_2H_2 (acetylene), the local quantum number is described by a single value
 7 ($L = J$, where J is the total angular momentum); for symmetric tops $L = (J, K, \ell)$ (e.g.
 8 C_2H_6); for molecules like HDO (a prolate asymmetric top) the structure is stored in a $E(J,$
 9 $K_a, K_c)$ array and the local quantum numbers would be $L = (J, K_a, K_c)$.

10

11 ***C.2. Computation of the partition function***

12 Computation of the total partition function (Q_{tot}) is particularly difficult, requiring
 13 complete knowledge of all electronic, vibrational, and rotational modes. In the seminal
 14 paper by Gamache et al. [1990], this problem was addressed for a limited set of linear
 15 molecules in the 70-3000K range; the first step in the development of the now widely
 16 used TIPS (Total Internal Partition Sums) program. This study has now been extended to
 17 the full database, and currently the HITRAN database provides total partition sums for all
 18 molecules and isotopologues present in the database for the 70-3000 K temperature range
 19 [Goldman et al. 2000, Fischer et al. 2003, see Pine and Rinsland 1999 for C_2H_6].

20 For temperatures lower than 70K, we have considered an analytical approach where we
 21 compute the vibrational and rotational partition functions independently. By using the
 22 retrieved rotational structure we compute the rotational partition function as:

$$Q_r = \sum_{i=L_{\min}}^{L_{\max}} w_i \exp(-c_2 E_i / T) \quad (\text{C-1})$$

For most molecules (not C₂H₆), the vibrational partition function for temperatures lower than 70K can be assumed to be unity, since they are only populated in their lowest vibrational/electronic level, and herewith the total partition function can be approximated to $Q_{\text{tot}} = Q_e Q_v Q_r \sim Q_r$ for low temps. In the case of C₂H₆ with a low-energy vibrational-level at $\sim 289 \text{ cm}^{-1}$ (Ev₄, torsional mode), we computed the vibrational partition for temperatures lower than 70K as following:

$$Q_{\text{vib}} = [1 - \exp(-c_2 E_{v_4} / T)]^{-1} \quad (\text{C-2})$$

C.3. Computation of fluorescence pumping rates

Perhaps one of the most valuable elements of spectral line lists is that the selection rules are explicitly defined by the existence (or non-existence) of a line. In addition, Hönl-London factors and Herman-Wallis effects (which are molecule and band dependent) are directly contained in the line intensities and A-coefficients. By iterating through the line atlas for each line, we compute the pumping rate ($g_{\text{pump}} [\text{s}^{-1}]$) from the reported A-coefficient (A_{21}), and add it to the corresponding upper-state population defined in L' (J',...) following [Crovisier and Encrenaz 1983, Weaver and Mumma 1984, Šimečková et al. 2006]:

$$g_{\text{pump}}(L') = \sum J_s(\nu_s) \cdot B_{12} \cdot w^s \exp(-c_2 E^s / T) / Q_{\text{tot}}(T) \quad (\text{C-3})$$

$$A_{\text{tot}}(L') = \sum A_{21} \quad (\text{C-4})$$

$$B_{12} = B_{21} \cdot \frac{w'}{w''} \quad (C-5)$$

$$B_{21} = A_{21} \cdot (8\pi h \nu^3)^{-1} \quad (C-6)$$

$$\nu_s = (1 - u/c)\nu \quad (C-7)$$

where J_s is the solar flux ($[J \text{ s cm}^{-3}]$, see Appendix B) at the Doppler shifted frequency ν_s of the line (being u $[cm \text{ s}^{-1}]$ the relative velocity between the comet and the sun and c the speed of light $[cm \text{ s}^{-1}]$), B_{12} the Einstein coefficient for induced absorption $[J^{-1} \text{ s}^{-2} \text{ cm}^3]$, B_{21} the Einstein coefficient for stimulated emission $[J^{-1} \text{ s}^{-2} \text{ cm}^3]$, A_{tot} the sum of Einstein A-coefficients $[s^{-1}]$ mapping to the upper state, and h is Planck's constant $[J \text{ s}]$.

9

10 ***C.4. Computation of fluorescence emission rates***

11 Once all pumps are computed, the branching ratios for each line 'i' are calculated as
12 A_{21}/A_{tot} , and with this cometary fluorescence rates (g-factor) are calculated as:

$$g_i = g_{pump}(L') \cdot \frac{A_{21}}{A_{tot}(L')} \quad (C-8)$$

14 Even though the branching ratios (A_{21}/A_{tot}) are temperature independent, the line-by-line
15 pumping rates (g_{pump}) are not, and thus g-factors must be computed for every line at the
16 appropriate temperature.